Biochemistry and Chemical Biology
Structural Biology and Molecular Biophysics

Kinetic regulation of kinesin's two motor domains coordinates its stepping along microtubules

Yamato Niitani, Kohei Matsuzaki, Erik Jonsson, Ronald D Vale, Michio Tomishige

Department of Applied Physics, School of Engineering, The University of Tokyo, Tokyo, Japan • Department of Physical Sciences, College of Science and Engineering, Aoyama Gakuin University, Sagamihara, Japan • Howard Hughes Medical Institute and Department of Cellular and Molecular Pharmacology, University of California, San Francisco, San Francisco, United States

Version of Record
April 17, 2025

Reviewed Preprint
v1 • March 24, 2025
Not revised

eLife Assessment

This study provides **compelling** evidence that kinesin's stepping mechanism is governed by strain-induced conformational changes in its nucleotide-binding pockets. Using pre-steady state kinetics and single-molecule assays, the authors demonstrate that the neck linker's conformation differentially modulates nucleotide affinity and detachment rates, establishing an asynchronous chemo-mechanical cycle that prevents simultaneous detachment. Supported by cryo-EM structural data, the work presents an **important** advance in our understanding of kinesin's hand-over-hand movement.

[Editors' note: this paper was reviewed by Review Commons.]

https://doi.org/10.7554/eLife.106228.1.sa4

Abstract

The two identical motor domains (heads) of dimeric kinesin-1 move in a hand-over-hand process along a microtubule, coordinating their ATPase cycles such that each ATP hydrolysis is tightly coupled to a step and enabling the motor to take many steps without dissociating. The neck linker, a structural element that connects the two heads, has been shown to be essential for the head-head coordination; however, which kinetic step(s) in the chemomechanical cycle is "gated" by the neck linker remains unresolved. Here, we employed pre-steady state kinetics and single molecule assays to investigate how the neck linker conformation affects kinesin's motility cycle. We show that the backward-pointing configuration of the neck linker in the front kinesin head confers higher affinity for microtubules, but does not change ATP binding and dissociation rates. In contrast, the forward-pointing configuration of the neck linker in the rear kinesin head decreases the ATP dissociation rate but has little effect on microtubule dissociation. In combination, these conformation-specific effects of the neck linker favor ATP hydrolysis and dissociation of the

rear head prior to microtubule detachment of the front head, thereby providing a kinetic explanation for the coordinated walking mechanism of dimeric kinesin.

Introduction

Kinesin-1 (hereafter called kinesin) is a dimeric motor protein that transports intracellular cargos by moving along microtubules. The unidirectional motion of kinesin toward the plus-end of the microtubule is driven by an N-terminal globular domain (termed "head") that catalyzes ATP hydrolysis and binds to the microtubule. The head is followed by a 14 amino-acid segment called the "neck linker" and then a long coiled-coil stalk that dimerizes the two identical polypeptide chains. Dimeric kinesin takes a 8 nm center-of-mass step by moving the rear head past the forward head along a microtubule protofilament once per ATP hydrolysis cycle; by alternating the movement of its two heads, kinesin can move processively for a micron or more without dissociating (Vale and Milligan, 2000; Asenjo et al., 2003; Kaseda et al., 2003; Asbury et al., 2003; Yildiz et al., 2004; Isojima et al., 2016; Wolff et al., 2023). The cycle of binding and dissociation of the head to/from the microtubule is tightly correlated with the ATPase cycle; release of ADP, creating a nucleotide-free state, stabilizes the microtubule binding of the head, while phosphate release after ATP hydrolysis induces detachment of the head from the microtubule (Gilbert and Johnson, 1994; Ma and Taylor, 1997a; Cross, 2004). Therefore, to alternately move the two heads, the ATP hydrolysis cycles in the rear and/or front heads should be differentially regulated ("gated"), such that the rear head hydrolyzes ATP and detaches from microtubule, prior to the front head (Hackney 1994; Ma and Taylor, 1997b; Gilbert et al., 1998; Auerbach and Johnson, 2005a; Cochran 2015).

To gate the ATPase cycles during processive movement, there must be a structural mechanism that enables the two heads to communicate with one another. When both heads are bound to the adjacent tubulin-binding sites ("two-head-bound state"), the front and rear heads are separated by 8 nm and cannot directly interact with each other. However, their neck linkers are highly extended and adopt two distinct configurations; the neck linker in the front head is stretched backward and the neck linker in the rear head is pointing forward, favoring the docked state (**Figure 1A**; Rice et al., 1999; Skiniotis et al., 2003; Tomishige et al., 2006; Liu et al., 2017). Artificially extending the neck linkers by inserting polypeptide spacers reduces the coupling ratio between forward step and ATP turnover, indicating that the strain transmitted through the neck linkers has an essential role for the head-head coordination (Hackney et al., 2003; Yildiz et al., 2008; Shastry and Hancock, 2010; Andreasson et al., 2015; Isojima et al., 2016).

Several models, which are not mutually exclusive, have been put forth to explain the alternating catalysis of the two heads and high coupling between ATP turnover and stepping (Block, 2007; Valentine and Gilbert, 2007; Gennerich and Vale, 2009). One type of model proposes neck linker-based regulation of microtubule affinity. A "rear-head gating" version of this model proposes that forward strain posed through neck linker accelerates the detachment of the rear head. Evidence supporting this model is based on experiments showing that the two-headed kinesin hydrolyzes ATP and detaches from microtubule much faster than a one-headed kinesin (Hancock and Howard, 1999; Crevel et al., 2004; Schief et al., 2004), and that the detachment rate of the head from microtubule is faster under a forward than a rearward pulling force from an optical trap (Uemura et al., 2002). However, other experimental results showed that the detachment rate from the microtubule by the rear head of a dimer or of the monomer under assisting load was not significantly accelerated (Rosenfeld et al., 2003; Andreasson et al., 2015; Dogan et al., 2015).

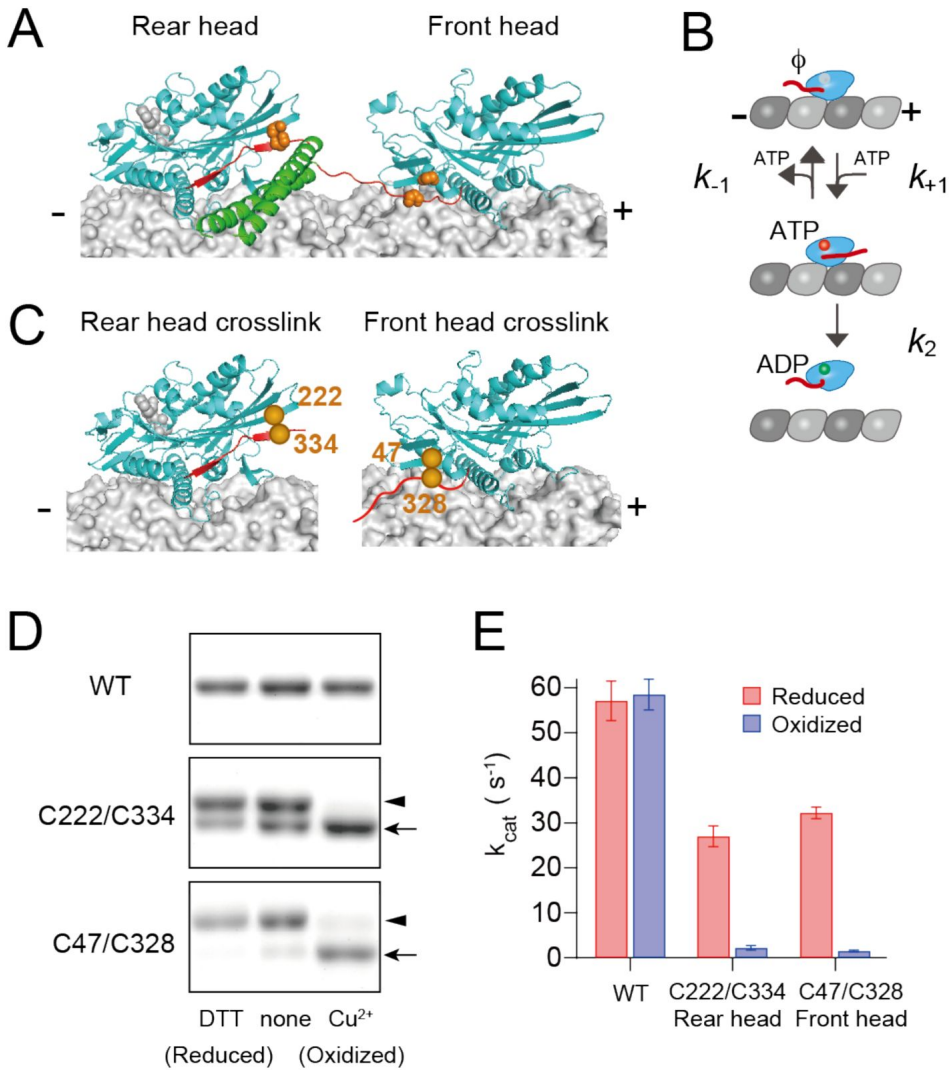

Figure 1.

Disulfide-crosslinking to constraint the neck linker in either the forward or backward pointing configuration.

(**A**) Three-dimensional structure of kinesin dimer on the microtubule in the two-head-bound intermediate state (modeled based on PDB# 4HNA and 4LNU). The motor domain, neck linker, and neck coiled-coil are shown in cyan, red, and green. Orange spheres represent the positions of cysteine residues as described in panel **C**. (**B**) Michaelis-Menten kinetics scheme for ATP-promoted dissociation of kinesin head from the microtubule, which includes ATP-binding (k_{+1}), ATP-dissociation (k_{-1}), and ATP-induced microtubule-dissociation (k_2) steps. (**C**) Positions of the cysteine residues for disulfide-crosslinking of monomeric kinesin. Cys222 and Cys334 were introduced to constrain the neck linker in the forward, docked conformation (left), while Cys47 and Cys328 were introduced to constrain the neck linker in the backward-pointing configuration (right). (**D**) Disulfide crosslinking after oxidative treatment was analyzed by nonreducing SDS-PAGE. WT (without Cys introduction), C222/C334, and C47/C328 constructs were treated with a reducing reagent (DTT), none, or oxidizing reagents (Cu^{2+}). Arrows and arrowheads indicate un-crosslinked and intramolecular crosslinked kinesins, respectively. The whole image of the gels is shown in Figure 1–figure supplement 1. (**E**) Microtubule-activated ATPase under reduced and oxidized conditions. k_{cat} and K_m(MT) were determined from the fit to a Michaelis-Menten equation of ATP turnover rates at various microtubule concentrations (Figure 1–figure supplement 2). Mean ± s.e.m. values were obtained from three independent assays.

Figure supplement 1. Estimation of disulfide-crosslinking efficiency.

Figure supplement 2. Steady-state microtubule-activated ATPase rates of monomeric kinesins before and after oxidative crosslinking.

Another class of gating models proposes that a chemical transition in the ATPase cycle is sensitive to neck linker tension between the two heads. A "front-head gating" model has been proposed that tension in the two-head bound state decreases ATP binding in the front head (Rosenfeld et al., 2003; Klumpp et al., 2004; Guydosh and Block, 2006; Dogan et al., 2015). Pre-steady state kinetic measurements showed that binding of mant-ATP (a fluorescent analogue that shows a signal change upon kinesin binding) to a microtubule-docked kinesin dimer showed single exponential kinetics with a signal amplitude nearly half than that expected if both heads can bind ATP (Rosenfeld et al., 2003; Klumpp et al., 2004). However, interpreting these results is complex, since the amplitude and duration of the mant-ATP signal is a composite from the front and rear heads, which complicates the assignment of specific rate constants of nucleotide binding and unbinding or isomerization events to the two microtubule-bound heads.

In this study, we measured the ATP-binding and microtubule-detachment kinetics (**Figure 1B**) of the front and rear heads separately using pre-steady state and single-molecule measurements. To isolate and measure the kinetics of the front and rear head states separately, we utilized two methods: 1) disulfide-crosslinking to immobilize the neck linker in monomeric kinesin in the forward- or backward-pointing configurations (mimicking the rear and front head states, respectively), and 2) a heterodimeric kinesin in which one polypeptide chain was locked in neck linker -docked, rear head conformation. Our results provide quantitative evidence that both kinesin heads participate in a coordinated gating mechanism: the backward constraint of the neck linker in the front head reduces its detachment rate from microtubules without changing ATP on/off-rates, while the forward constraint on the neck linker in the rear head dramatically reduces ATP dissociation rate but has minimal effect on microtubule affinity. These results are consistent with the open and closed conformations of the nucleotide-binding pocket in the front and rear heads of microtubule-bound kinesin dimers observed in cryo-electron microscopy (cryo-EM) studies (Liu et al., 2017; Benoit et al., 2021) and provide a mechanism for the coordinated hand-over-hand movement of kinesin.

Results

Controlling the neck-linker orientation of monomer kinesin through crosslinking

We first sought to examine the kinetics of nucleotide binding and microtubule dissociation of monomeric kinesin in which the neck linker was oriented either in the forward (mimicking the rear head) or the rearward (mimicking the front head) direction (**Figure 1A, C**). To control the orientation of the neck linker in monomer kinesin, we employed disulfide-crosslink between two cysteines, one on the head and the other on the neck linker (Tomishige and Vale, 2000). To immobilize the neck linker in this forward-pointing, docked conformation (Gigant et al., 2013), K222 (located at the plus-end oriented tip of the head) and E334 (the distal end of the docked neck linker) residues were substituted with cysteines in a Cys-light monomeric kinesin (K339 Cys-light), whose solvent-exposed cysteines were replaced by either Ser or Ala (Rice et al., 1999) (**Figure 1C**, left). We refer to the C222/C334 crosslink here as "rear head crosslink". We previously introduced this cysteine pair into dimeric kinesin and found that oxidative crosslinking resulted in a complete loss of directionality (Tomishige and Vale, 2000). The neck linker of the front head is detached from the head, and its distal end is pulled backward (Skiniotis et al., 2003; Tomishige et al., 2006; Benoit et al., 2021). To constrain the neck linker in this backward-pointing configuration, which we refer to as the "front head crosslink", A47 (the minus-end-oriented base of the head) and T328 (five residues from the proximal end of the neck linker) residues were substituted with cysteines (**Figure 1C**, right). The cysteine pairs were covalently crosslinked by oxidative treatment with copper ion and o-phenanthroline (Kobashi, 1968; Kaan et al., 2011).

The crosslinking efficiencies were estimated, by running SDS-PAGE under non-reducing conditions, to be 97% and 87% for the rear and front head crosslinks, respectively (**Figure 1D** and **Figure 1–figure supplement 1**).

We first evaluated the effect of disulfide crosslinking on the microtubule-activated ATP turnover rates (**Figure 1–figure supplement 2**). Under reducing conditions, the k_{cat} for both the rear and front head crosslinks (27.0 and 32.2 ATP/s per head, respectively) were lower than WT (57.1 ATP/s per head) (**Figure 1E**). The reduced ATPase activity primarily results from a decreased microtubule association rate (data to be presented elsewhere) with little change in ATP binding or microtubule dissociation rates (**Table 1**). For the rear head crosslink, the reduced ATPase activity might also be due to the presence of crosslinked species even under the reducing condition (~30%; **Figure 1D** and **Figure 1–figure supplement 1B**). Under oxidized conditions, the k_{cat} values for both rear and front head crosslinks were reduced by more than 10-fold compared to that under reducing condition (2.2 and 1.5 ATP/s per head, respectively (**Figure 1E** and **Table 1**)). These results demonstrate that neck linker constraints in both forward and rearward orientations inhibit specific steps in the mechanochemical cycle of the head.

Effect of neck linker crosslinking on the binding/dissociation rates of ATP

To measure ATP binding rate to kinesin head on the microtubule, we rapidly mixed the nucleotide-free kinesin-microtubule complex with increasing concentrations of mant-ATP using stopped flow apparatus. The initial rapid increase in the fluorescence represents mant-ATP binding to the nucleotide pocket of the motor domain; this rapidly increasing phase was fit with an exponential to obtain the observed rate k_{obs} (**Figure 2–figure supplement 1**). At low mant-ATP concentrations, the k_{obs} increased linearly as a function of mant-ATP concentration (Ma and Taylor, 1997a; Moyer et al., 1998); the slope of the fitted line provides the binding rate k_{+1} and the offset provides the dissociation rate k_{-1} (**Figure 2A**). First, we demonstrated that k_{+1} and k_{-1} of the wild-type head without Cys-modification were unchanged after oxidization (**Table 1**) and were comparable to those previously reported (Cross, 2004). Rear head crosslinking resulted in a modest decrease in the on-rate k_{+1} by three-fold (5.1 and 1.6 $s^{-1}\mu M^{-1}$ under reducing and oxidizing conditions, respectively; **Figure 2B**). However, rear head crosslinking produced a 30-fold decrease in the off-rate k_{-1} (117 and 3.7 s^{-1} under reducing and oxidizing conditions, respectively). In contrast, front head crosslinking resulted in only a modest and similar 2-fold decrease in both k_{+1} and k_{-1} (k_{+1} was 4.0 and 2.0 $s^{-1}\mu M^{-1}$, k_{-1} was 96 and 42 s^{-1} under reducing and oxidizing conditions, respectively; **Figure 2B**), resulting in little or no change in the affinity for ATP after crosslinking. These results indicate that the rear head crosslink reduces the ATP dissociation rate, while the front head crosslink does not significantly alter the ATP binding kinetics. We note that the measured k_{-1} of rear head crosslink was similar to the ATP turnover rate k_{cat} (**Table 1**); therefore, it is likely that the majority of ATP molecules bound to the head were hydrolyzed, and the observed fluorescence decrease rather represents mant-ADP release.

To detect the ATP dissociation event of the rear head, we employed a mutant kinesin with a point mutation of E236A in the switch II loop, which almost abolishes ATPase hydrolysis and traps in the microtubule-bound, neck-linker docked state (Rice et al., 1999; Auerbach and Johnson, 2005b). The mant-ATP binding kinetics of E236A monomer revealed an ATP on-rate (k_{+1} of 5.6 $s^{-1}\mu M^{-1}$) comparable to that of wild-type monomer (6.6 $s^{-1}\mu M^{-1}$), indicating that the initial ATP-binding step remains unaffected by the mutation (**Figure 2C** and **Figure 2–figure supplement 2**). The ATP off-rate could not be precisely determined from the offset value of the linear fitting of the k_{obs} plot due to its small magnitude.

			Rear head		Front head	
	WT		C222/C334		C47/C328	
	Reduced	Oxidized	Reduced	Oxidized	Reduced	Oxidized
k_{cat} (s^{-1})	57.1 ± 4.4	58.5 ± 3.4	27.0 ± 2.3	2.2 ± 0.5	32.2 ± 1.3	1.5 ± 0.2
K_m(MT) (μM)	0.31 ± 0.08	0.36 ± 0.08	0.23 ± 0.06	0.200 ± 0.007	0.28 ± 0.06	0.13 ± 0.04
k_{+1} ($s^{-1}μM^{-1}$)	5.5 ± 0.1	6.0 ± 0.4	5.1 ± 0.7	1.62 ± 0.07	4.0 ± 0.2	2.0 ± 0.1
k_{-1} (s^{-1})	136 ± 5	125 ± 12	117 ± 23	3.7 ± 1.9	96 ± 6	42 ± 4
k_2 (s^{-1})	52.1 ± 0.6	59.1 ± 0.9	69.3 ± 0.5	N.D.	51.5 ± 0.7	7.0 ± 0.3
k_{2_SMF} (s^{-1})	44.0 ± 1.9	41.6 ± 1.2	47.2 ± 1.2	57.1 ± 2.3	42.1 ± 0.4	2.30 ± 0.08

	C4/C330		C47/C335	
	Reduced	Oxidized	Reduced	Oxidized
k_{cat} (s^{-1})	33.5 ± 2.1	32.6 ± 1.2	43.1 ± 3.0	11.9 ± 0.6
K_m(MT) (μM)	0.42 ± 0.08	8.36 ± 0.98	0.33 ± 0.05	0.10 ± 0.01
k_{+1} ($s^{-1}μM^{-1}$)	4.7 ± 0.5	4.1 ± 0.3	9.1 ± 0.3	4.5 ± 0.1
k_{-1} (s^{-1})	148 ± 18	96 ± 9	85 ± 10	41 ± 5
k_2 (s^{-1})	68.6 ± 0.5	80.8 ± 0.8	41.6 ± 0.6	19.4 ± 0.2
k_{2_SMF} (s^{-1})	59.5 ± 2.3	58.4 ± 2.6	52.1 ± 2.0	22.5 ± 0.3

Table 1.

Kinetic rate constants for disulfide-crosslinking monomers. Steady-state ATP-turnover rate (k_{cat} and K_m(MT)), pre-steady-state mant-ATP binding (k_{+1} and k_{-1}) and microtubule dissociation rates (k_2 and k_{2_SMF}, measured by light scattering and single-molecule fluorescence) measured under reduced and oxidized conditions.

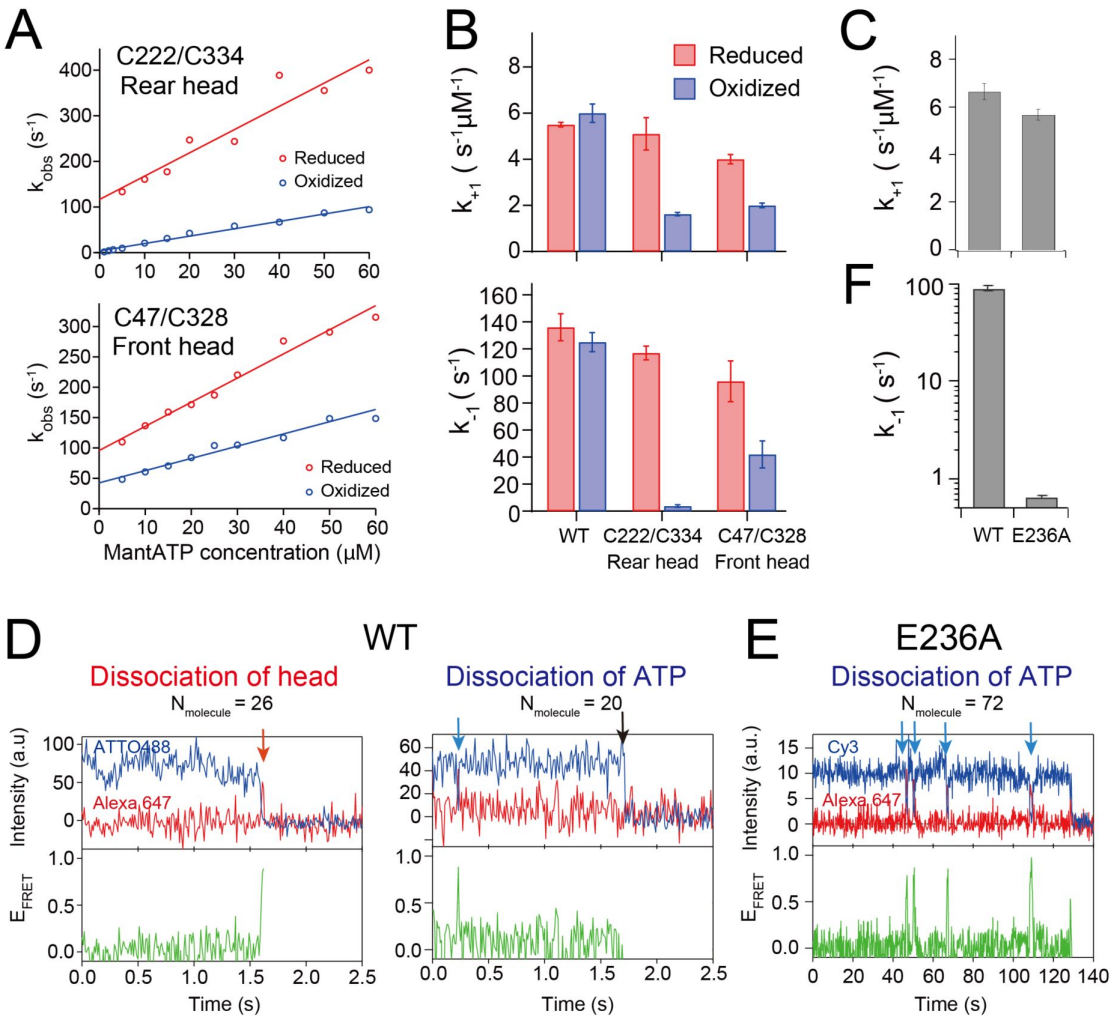

Figure 2.

ATP-binding/dissociation kinetics of disulfide-crosslinked monomers.

(**A**) The rate of initial enhancement of the fluorescence after rapid mixing of kinesin-microtubule complex with mant-ATP (k_{obs}; **Figure 2–figure supplement 1**) was plotted as a function of mant-ATP concentration. Solid lines represent a linear fit; the slope provides the on-rate of mant-ATP (k_{+1}) and the off-set provides the off-rate of mant-ATP (k_{-1}). (**B**) ATP binding rate k_{+1} and ATP dissociation rate k_{-1} of monomers before and after crosslinking obtained from the fit shown in pane **A**. Error bar shows the fit error. (**C**) Mant-dATP binding rate k_{+1} to wild-type (WT) and E236A monomers (k_{obs} plots are shown in **Figure 2–figure supplement 2**). (**D**) Two typical traces of smFRET between the donor-labeled wild-type monomer and Alexa-ATP (500 nM). Fluorescence intensities of donor (blue) and acceptor (red), and the calculated FRET efficiency (green) recorded at 100 fps are shown. Left trace: the FRET efficiency transiently increases just before both dyes disappear (indicated by the red arrow), suggesting that the nucleotide-bound head detached from the microtubule (**Figure 2–figure supplement 4A**). Right trace: the FRET efficiency transiently increases, followed by the recovery of donor fluorescent (shown by the blue arrow), indicating the reversible dissociation of ATP. The black arrow indicates the photobleaching of the donor dye. The numbers of molecules observed for each type is shown at the top of the traces. (**E**) Typical trace of smFRET between the E236A monomer and Alexa-ATP (200 nM) recorded at 5 fps, demonstrating repetitive ATP binding and dissociation. (**F**) The dissociation rate k_{-1} of Alexa-ATP from wild-type and E236A monomers (histograms are shown in **Figure 2–figure supplement 4B**). The value for the wild-type may be underestimated due to the limited temporal resolution (10 ms).

Figure supplement 1. Pre-steady-state kinetics of ATP binding to monomeric kinesin-microtubule complex before and after crosslinking.

Figure supplement 2. ATP binding kinetics for E236A mutant monomer on microtubule. **Figure supplement 3**. Processive motility of wild-type kinesin dimer driven by Alexa 647 ATP.

Figure supplement 4. Dwell time of Alexa-ATP-bound state for wild-type and E236A monomers determined using smFRET.

To determine the ATP off-rate k_{-1} of E236A monomer, we employed single-molecule fluorescence resonance energy transfer (smFRET) between the donor dye attached to the head and the acceptor dye conjugated to ATP. The residue S55, separated by ~0.8 nm from the nucleotide pocket, was substituted with cysteine and was labeled with ATTO488 or Cy3 dye; we would expect ~90% high FRET efficiency when Alexa 647-conjugated ATP (termed as Alexa-ATP) binds to the labeled head (**Figure 2–figure supplement 4A**). Using wild-type kinesin dimer, we demonstrated that Alexa-ATP acts as a substrate to drive kinesin motility along microtubule, although velocities were about 10-fold lower than those driven by unmodified ATP (**Figure 2–figure supplement 3**). First, we observed single-molecule FRET of ATTO488-labeled "wild-type" monomer on microtubule in the presence of 500 nM Alexa-ATP. We observed FRET efficiency increases upon Alexa-ATP binding to microtubule-bound monomer, and then the donor and acceptor simultaneously disappeared (representing that the head dissociated from microtubule after ATP hydrolysis; **Figure 2D**, left), or the donor fluorescence recovered after disappearance of the acceptor fluorescence (representing that ATP dissociated while the head remains bound to the microtubule; **Figure 2D**, right). We found that the ATP bound to wild-type head could be either hydrolyzed, followed by head dissociation from the microtubule, or reversibly dissociated with nearly equal probability (**Figure 2D**). This finding is consistent with the mant-ATP binding kinetics measurements of the monomer without neck-linker constraint, which showed similar k_2 and k_{-1} values (**Table 1**). In contrast, the single-molecule FRET observation of Cy3-labeled E236A monomer in the presence of 200 nM Alexa-ATP showed that the majority of the Cy3-labeled mutant remained bound to the microtubule during the observation period, and Alexa-ATP molecules repeatedly bound and reversibly dissociated to/from the mutant head (**Figure 2E**). The mean dwell time of the high FRET state (ATP-bound state) was 1.54 s, which corresponds to k_{-1} of 0.65 s^{-1} (**Figure 2F** and **Figure 2–figure supplement 4B**), a value 140-fold smaller than that of the wild-type monomer (91 s^{-1}). We note that the neck linker of the E236A monomer was neither pulled forward nor constrained by crosslinking; therefore, the ATP off-rate of monomeric E236A may still be faster than that of the rear head in dimeric kinesin (as will be examined later).

Effect of neck linker crosslinking on the dissociation rate from microtubule

Next, we analyzed the effect of the neck-linker crosslinking on the detachment rate of the monomeric kinesin from microtubule (MT dissociation). First, we measured turbidity change after rapidly mixing the nucleotide-free kinesin-microtubule complex with 1 mM ATP using stopped-flow apparatus. Since monomeric kinesin repeatedly hydrolyzes ATP per encounter to the microtubule through electrostatic interactions (Jiang and Hackney, 1997), we included 150 mM KCl to prevent reassociation of the detached head. However, the rear head crosslink kinesin did not show any initial burst in turbidity after oxidative treatment (Figure 3–figure supplement 1), because this constraint on the neck linker dramatically reduces the microtubule-activated ADP release rate (data to be presented elsewhere), creating a weak microtubule binding state. In contrast, the front head crosslink kinesin displayed an initial burst phase for MT dissociation under these salt conditions. The fit of the initial decay revealed a 7-fold decrease in the MT dissociation rate k_2 (51.5 and 7.0 s^{-1} for reduced and oxidized conditions, respectively (**Figure 3A**)).

Since we could not measure the MT dissociation for the rear head using light scattering, we sought an alternate approach involving visualizing GFP-fused K339 Cys-light kinesin binding to the microtubule using single-molecule fluorescent microscopy in the presence of 100 mM KCl and 1 mM ATP (**Figure 3B**). The rear head crosslink showed a 6-fold reduced binding frequency to microtubule (**Figure 3–figure supplement 2A**). We fit the histograms of the dwell time of fluorescent spots on microtubule with single exponential decay (**Figure 3–figure supplement 2B**) and employed the inverse of the dwell time as a rough estimate of the dissociation rate (termed as k_{2_SMF}). The k_{2_SMF} of the rear head crosslink was slightly increased compared to before crosslinking (47.2 and 57.1 s^{-1} under reducing and oxidizing conditions, respectively). In

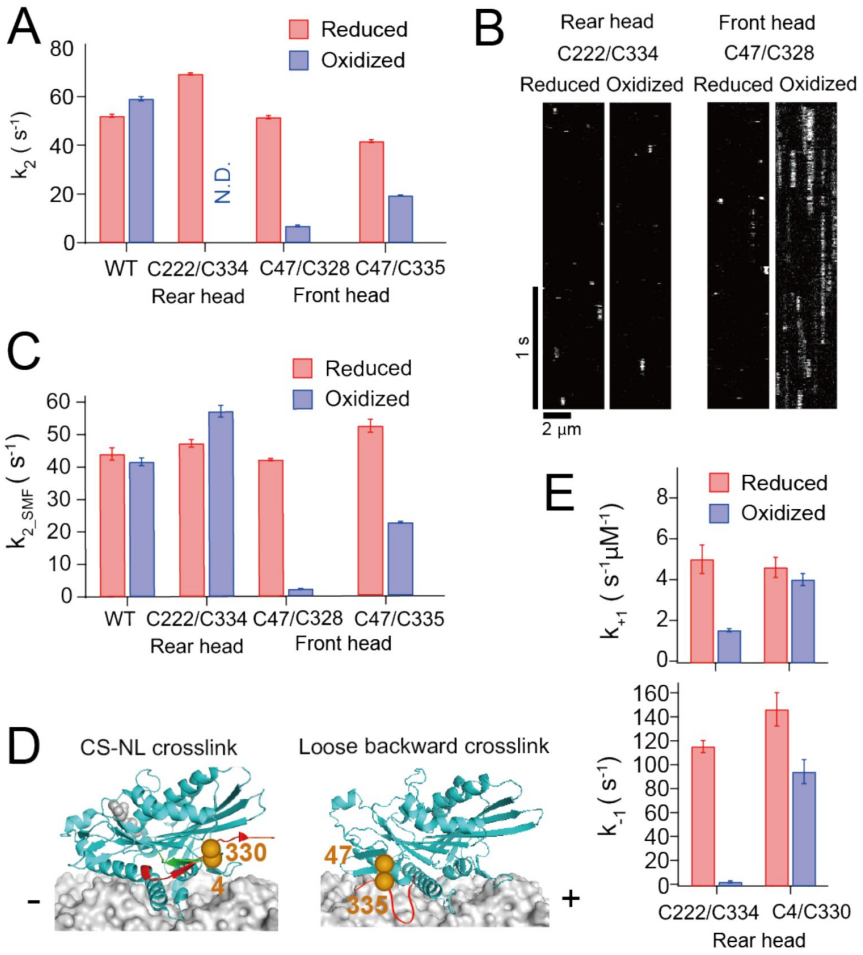

Figure 3.

Microtubule-detachment kinetics of disulfide-crosslinked monomers.

(**A**) ATP-induced dissociation rate from microtubule k_2 measured by turbidity change after the rapid mixing of kinesin-microtubule complex with 1 mM ATP. The turbidity time traces are shown in **Figure 3–figure supplement 1**. (**B**) Kymographs showing the binding and dissociation of GFP-fused kinesin under reduced and oxidized conditions on the microtubule. C47/C328 showed an extended dwell on the microtubule after crosslinking. (**C**) ATP-induced dissociation rate from the microtubule measured using single-molecule observations of GFP-fused kinesin. k_{2_SMF} was determined as an inverse of the mean dwell time of the fluorescent kinesin on the microtubule in the presence of 1 mM ATP. The dwell time histograms are shown in **Figure 3–figure supplement 2B**. (**D**) Positions of Cys4 and Cys330 residues for disulfide-crosslinking of a monomer between the N-terminal cover strand (CS; green) and the neck linker (NL; red) (left). Positions of Cys47 and Cys335 residues for disulfide-crosslinking of a monomer to constrain the neck linker in the backward-pointing configuration allowing partial docking of the neck linker (right; **Figure 3–figure supplement 3**). The ATP-induced dissociation rates from the microtubule of C47/C335 monomer before and after crosslinking, measured by turbidity change (k_2) and single-molecule fluorescence (k_{2_SMF}), are shown in **Figure 3A, C**. Histograms are displayed in **Figure 3–figure supplement 4E**. (**E**) Mant-ATP binding rate k_{+1} and dissociation rate k_{-1} of C4/C330 monomer before and after crosslinking (data for C222/C334 are included from **Figure 2B** for comparison). The k_{obs} plots are shown in **Figure 3–figure supplement 4B**.

Figure supplement 1. ATP-induced dissociation kinetics of crosslinked kinesin from microtubule measured using light scattering.

Figure supplement 2. ATP-dependent microtubule-binding and -dissociation of crosslinked kinesins observed by single-molecule fluorescence microscopy.

Figure supplement 3. Locations of the C47/C328 and C47/C335 residues when the labeled head is in the front or rear of dimeric kinesin.

Figure supplement 4. Kinetics measurements of ATP-binding and microtubule-dissociation of C4/C330 and C47/C335 crosslinked monomeric kinesins.

contrast, the front head crosslink showed an 18-fold decrease in the k_{2_SMF} compared to before crosslinking (42.1 and 2.3 s^{-1} under reducing and oxidizing conditions, respectively) (**Figure 3C** and **Table 1**). These results suggest that forward constraint on the neck linker in the rear head does not significantly accelerate the detachment from microtubule, while backward constraint of the neck linker in the front head reduces the detachment rate.

Different crosslinking schemes to examine the role of the neck-linker docking on gating

The reduced detachment rate of the front head crosslink is likely due to the inability of the C47/C328 crosslinked head to adopt the neck-linker docked conformation. Then, we asked whether the reduced detachment rate can be recovered if the crosslinked neck linker is allowed to partially dock onto the head. To test this, we crosslinked the neck linker in the backward orientation between C47 on the head and C335 on the neck linker (**Figure 3D**, right), which produces an extra 7 amino acids compared to C47/C328 between the base and the crosslinked residues on the neck linker, allowing the initial few residues of the neck linker (including I325 residue involved in filling the hydrophobic pocket exposed on the ATP-bound head (Vale and Milligan, 2000; Sindelar, 2011; Cao et al., 2014)) to dock onto the head (Figure 3–figure supplement 3). The ATP-induced detachment rate k_2 of C47/C335 showed only two-fold reduction after crosslinking (41.6 and 19.4 s^{-1} for reduced and oxidized conditions, respectively, measured using light scattering; **Figure 3A, C** and **Figure 3–figure supplement 4C-E**). This finding is consistent with the idea that the gatekeeper of the front head gate is the neck-linker docking and suggests that partial neck linker docking onto the head is sufficient to half open the gate, while more extensive neck linker docking is required to fully open the gate.

In contrast, the neck linker orientation in the rear head crosslink did not change the dissociation rate from microtubules but reduced the dissociation rate of ATP (**Figure 2B**). We examined an alternate crosslinking scheme between C4 on the N-terminal stretch and C330 on the neck linker (Tomishige and Vale, 2000), which couples the neck linker (NL) with the N-terminal flexible segment called “cover strand (CS)” (**Figure 3D**, left). The interaction between the neck linker and cover strand has been shown to be important to produce a forward-bias in the diffusional motion of the detached head against hindering load (Hwang et al., 2008; Khalil et al., 2008). The ATP dissociation rate k_{-1} was not significantly affected by C4/C330 crosslinking (148^{-1} and 96 s^{-1} for reduced and oxidized conditions, respectively; **Figure 3E** and **Figure 3–figure supplement 4B**), indicating that the interaction of the neck linker with the head, not with the N-terminal cover strand, is responsible for the reduction of the ATP off-rate.

A E236A-WT heterodimer to distinguish front and rear heads

The front head crosslink was designed to constrain the neck linker to mimic the neck linker orientation of the front head. However, it differs from that of the front head in that the backward-pointing configuration is maintained by the crosslinking, not by the backward strain originating from the stretched neck linkers between two microtubule-bound heads (Hyeon and Onuchic, 2007; Hariharan and Hancock, 2009). We sought to further investigate how the neck linker tension contributes to the front head gating by examining the nucleotide-binding and microtubule detachment kinetics of the front head in the context of a dimeric kinesin. To this end, we employed a heterodimer in which one polypeptide is wild-type (WT) and the other contains the E236A mutation (E236A-WT heterodimer). As described above, E236A mutant acts as a long-lived rear head, which is kinetically trapped in the neck-linker docked, pre-ATP hydrolysis state. Thus, in the E236A-WT heterodimer in the presence of ATP, one would expect the E236A head to be in the rear and the WT head to occupy the front.

To test this assumption, we used the smFRET sensor, which has been used to distinguish the configurations of two heads (Mori et al., 2007). We first introduced one cysteine into the residue 215 (located at the plus-end oriented tip of the head) of the E236A chain and another into the

residue 43 (located at the minus-end oriented base of the head) of WT chain and labeled with Cy3 and Cy5 fluorophores (Figure 4–figure supplement 1, left). The FRET efficiency of dual-labeled molecules bound to the microtubule in the presence of ATP showed a single peak at about 90%. When we introduced 43Cys into the E236A chain and 215Cys into the WT chain, however, the distribution of the FRET efficiency showed a single peak at about 10% (Figure 4–figure supplement 1, right). These results are consistent with E236A-WT heterodimer stably taking two-head-bound state, in which WT head is in the front and E236A head is in the rear position.

ATP binding kinetics of the front and rear heads of the heterodimer

First, we measured the steady-state microtubule-activated ATPase activity of the E236A-WT heterodimer. The microtubule-activated ATPase k_{cat} of the E236A-WT heterodimer was 4.6 ATP/s per head (Figure 6–figure supplement 1), suggesting that the front WT head is capable of hydrolyzing ATP, but its catalytic activity is suppressed (c.f. ~30 ATP/s per head for wild-type dimer (Tomishige and Vale, 2000)). As described later, the reduced ATPase rate results from suppressed microtubule detachment of the front WT head, while the rear E236A head is virtually unable to detach from microtubules.

Next, we measured ATP-binding kinetics of the wild-type front head in the E236A-WT heterodimer using a stopped-flow apparatus. To selectively observe fluorescent signal of mant-ATP bound to the wild-type front head, we quenched the fluorescent signal of mant-ATP bound to the E236A head by substituting residue H100 (located in loop 5 near the nucleotide pocket) in the E236A chain with cysteine and labeling it with Alexa 488 dye, which acts as an acceptor for mant-ATP (**Figure 4A**, upper). The measured ATP on-rate k_{+1} and off-rate k_{-1} were 5.3 $\mu M^{-1}s^{-1}$ and 92 s^{-1}, respectively (**Figure 4B, C, F** and **Figure 4–figure supplement 2**), which were similar to those of the un-crosslinked monomer (**Figure 2C, F**). These results further support the notion that ATP binding kinetics of the front head are not significantly affected by the backward strain posed to the neck linker.

We also measured ATP-binding kinetics of the E236A rear head of the heterodimer. Pre-steady state kinetic measurements using E236A-WT heterodimer with Alexa 488 modification on the wild-type head (**Figure 4A**, lower) revealed an ATP on-rate k_{+1} of 4.4 $\mu M^{-1}s^{-1}$ (**Figure 4B, C** and **Figure 4–figure supplement 2**), similar to that of un-crosslinked WT and E236A monomers (**Figure 2C**). Since the ATP off-rate k_{-1} could not be accurately measured using stopped-flow (k_{-1} was −3.3 s^{-1}), we used smFRET between a donor Cy3 on the E236A rear head (with cysteine modification at S43) and an acceptor Alexa-ATP. We expected ~80% high FRET when Alexa-ATP bound to the rear E236A head (dye distance ~2.5 nm; **Figure 4D**, upper) and low FRET when ATP bound to the front wild-type head (dye distance ~9 nm; **Figure 4D**, lower). The high FRET state showed a mean dwell time of 65.5 s, corresponding to k_{-1} of 0.015 s^{-1} (**Figure 4E, F** and **Figure 4–figure supplement 3**). This ATP off-rate is 42-fold smaller than that of the E236A monomer (**Figure 2E, F**), indicating that forward strain prevents nucleotide release.

Microtubule detachment rate of the front head of E236A-WT heterodimer

Next, we measured ATP-induced detachment rate k_2 of the front WT head of E236A-WT heterodimer from the microtubule using high-speed single-molecule microscopy (**Figure 5A**; Isojima et al., 2016). We labeled WT head with a gold nanoparticle (40 nm in diameter) and observed the motion of the gold probe attached to E236A-WT heterodimer on the microtubule in the presence of 1 mM ATP. With the temporal resolution of the measurement (50 μs), we could clearly identify transient increases in the fluctuation of the gold probe accompanied by detachment of the labeled head (**Figure 5B**). Moreover, these observations allowed us to distinguish whether the gold-labeled WT head was in the leading or trailing position just before

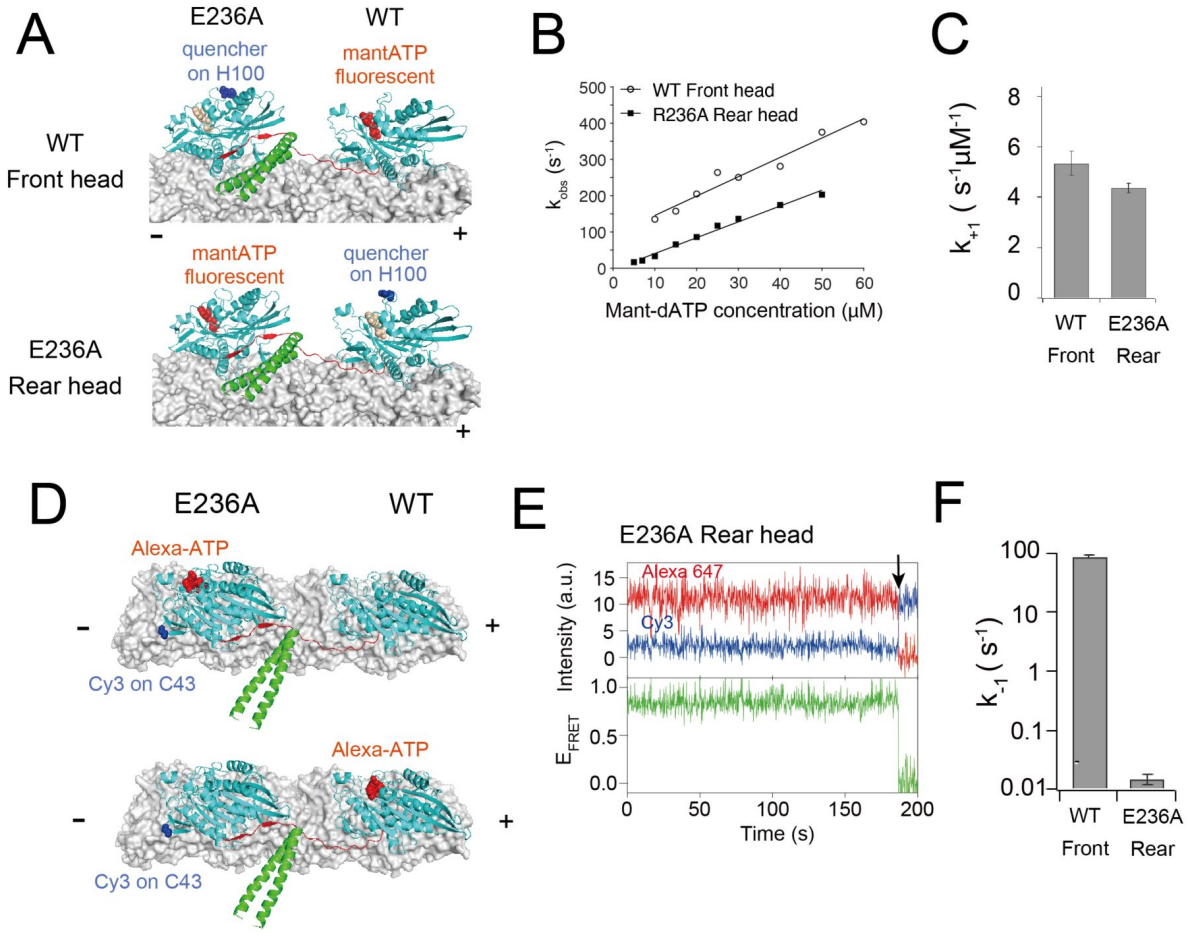

Figure 4.

ATP-binding/dissociation kinetics of the E236A-WT heterodimer.

(**A**) Diagram showing the positions of H100 residue (highlighted in blue) labeled with Alexa 488 dye. This label quenches the mant-ATP signal of either the rear W236A head (upper; used to measure ATP-binding to the front head) or the front wild-type head (lower; used to measure ATP-binding to the rear head). (**B**) k_{obs} plots for mant-ATP binding to the front wild-type and rear E236A heads of the E236A-WT heterodimer (typical fluorescent transients are shown in **Figure 4–figure supplement 2**). Solid lines indicate a linear fit. The fit parameters are k_{+1} = 5.3 ± 0.5 $\mu M^{-1}s^{-1}$ and k_{-1} = 92 ± 16 s^{-1} for WT front head and k_{+1} = 4.4 ± 0.2 $\mu M^{-1}s^{-1}$ and k_{-1} = −3.3 ± 5.1 s^{-1} for E236A rear head. (**C**) ATP-binding rate (k_{+1}) for front and rear heads of the E236A-WT heterodimer, as determined by fitting in panel **B**. Diagram showing the position of Cys43 residue of E236A chain for labeling with donor (Cy3; blue) fluorophore, and the Alexa 647 ATP (red) bound to the rear E236A head (upper) or the front wild-type head (lower) of the E236A-WT heterodimer. High FRET efficiency is expected when the Alexa-ATP binds specifically to the rear E236A head. (**E**) A representative trace of fluorescence intensities of donor (Cy3; blue) on the E236A rear head and acceptor (Alexa 647; red) fluorophores, with calculated FRET efficiency (green), for the E236A-WT heterodimer at 200 nM Alexa-ATP recorded at 5 fps. The black arrow indicates the dissociation of Alexa-ATP, accompanied by the recovery of donor fluorescent. ATP remained bound to the rear head significantly longer compared to the E236A monomer (**Figure 2E**). (**F**) ATP dissociation rate (k_{-1}) for front and rear heads of the E236A-WT heterodimer. Note that these rates were measured using different methods (stopped flow for the WT font head (**Figure 4B**) and smFRET for the E236A rear head (**Figure 4E**)) and thus cannot be directly compared.

Figure supplement 1. Single-molecule FRET between two heads of E236A-WT heterodimer. **Figure supplement 2**. ATP binding kinetics for front and rear heads of E236A-WT heterodimer.

Figure supplement 3. Single-molecule FRET observation between donor dye on one of the head of E236A-WT heterodimer and acceptor-labeled ATP.

microtubule detachment; the backward displacement of the detached head indicates that the labeled WT head occupied the leading position prior to detachment (**Figure 5–figure supplement 1**). Unlike the unbound trailing head of wild-type dimer that showed continuous mobility (Isojima et al., 2016), the unbound WT head of E236A-WT heterodimer exhibited a low-fluctuation state in the middle (**Figure 5B**, s.d. traces). This low-fluctuation unbound state was distinguishable from the typical microtubule-bound state, having a shorter dwell time of ~5 ms compared to the bound state and positioning backward, closer to the E236A head, relative to the bound state (**Figure 5–figure supplement 2**). The mean dwell time of the bound and unbound states of the front head at 1 mM ATP was 160 and 11 ms, respectively (**Figure 5C** and **Figure 5–figure supplement 3**).

To determine the rate constants for the ATP-promoted detachment rate of the front WT head, we measured the dwell time of microtubule-bound state of the gold-labeled WT head under various ATP conditions (**Figure 5D** and **Figure 5–figure supplement 3**). The mean dwell time increased as ATP concentration was decreased (**Figure 5E**), indicating that the bound dwell time includes ATP-binding and hydrolysis in the front head. The inverse of the mean dwell time plotted against ATP concentration could be well fit with a Michaelis-Menten equation with fit parameters of k_{cat} = 6.3 ± 0.2 s^{-1} and K_m = 43 ± 6 μM (**Figure 6D**). The observed k_{cat} also includes ADP release rate; however, since ADP release (~5 ms) becomes negligible within the dwell time of >160 ms, we took this k_{cat} as an approximation of the ATP-promoted detachment rate k_2. The k_2 determined using E236A-WT heterodimer (6.3 s^{-1}) is similar to the k_2 of front head crosslink (7.0 s^{-1}), supporting the notion that the backward strain posed to the neck linker significantly reduces nucleotide-induced detachment rate of the front head. In contrast, the dwell time of the unbound state of the gold-labeled WT head showed weak ATP dependence (**Figure 5–figure supplement 2**), indicating that the rear E236A head occasionally releases ATP when the front head detaches from the microtubule and the neck linker of E236A head becomes unconstrainted. This finding further supports the idea that forward neck linker strain plays a crucial role in reducing the reversible ATP release rate.

Effect of the neck-linker tension on the gating of the front and rear heads

Experimental results obtained from neck-linker crosslinking monomers and the E236A-WT heterodimer revealed that distinct chemical steps are gated in the front and rear heads (k_2 and k_{-1} respectively). We next sought to examine whether neck linker tension places a role in gating these steps. To reduce the tension posed to the neck linker in the two-head-bound state, we extended the neck linker of E236A-WT heterodimer by inserting 7 or 12 glycine residues between neck linker and neck coiled-coil of both chains (referred to as G7 and G12) (**Figure 6A**; Isojima et al., 2016). The microtubule-activated ATPase rate of G12 increased modestly by 1.6-fold compared to that of the heterodimer without neck-linker extension (referred to as G0) (**Figure 6B** and **Figure 6–figure supplement 1**).

We first examined the effect of the tension posed to the neck linker on ATP-induced detachment rate k_2 of the front head, by observing the neck-linker extended E236A-WT heterodimer using high-speed dark-field microscopy. The gold probe attached to the front WT head of G7 and G12 heterodimers showed transient increases in the fluctuation of the gold probe (**Figure 6C**). The inverse of the dwell time of bound state for G7 and G12 mutants (**Figure 6–figure supplement 2, 3**) plotted against ATP concentration fit well with the Michaelis-Menten equation (**Figure 6D**); the fit parameters are k_{cat} = 7.6 ± 0.9 s^{-1} and K_m = 22 ± 10 μM for G7 and k_{cat} = 9.3 ± 0.7 s^{-1} and K_m = 6.1 ± 2.1 μM for G12. The k_2 modestly increased as the inserted poly-Gly number increased; G12 showed 1.5-fold increase in k_2 compared to G0 (**Figure 6E**), reminiscent of the results of ATPase rates (**Figure 6B**). The detached WT head of G12 heterodimer occasionally bound to the rear-tubulin binding site (the frequency was 14% among all binding events); however, the head

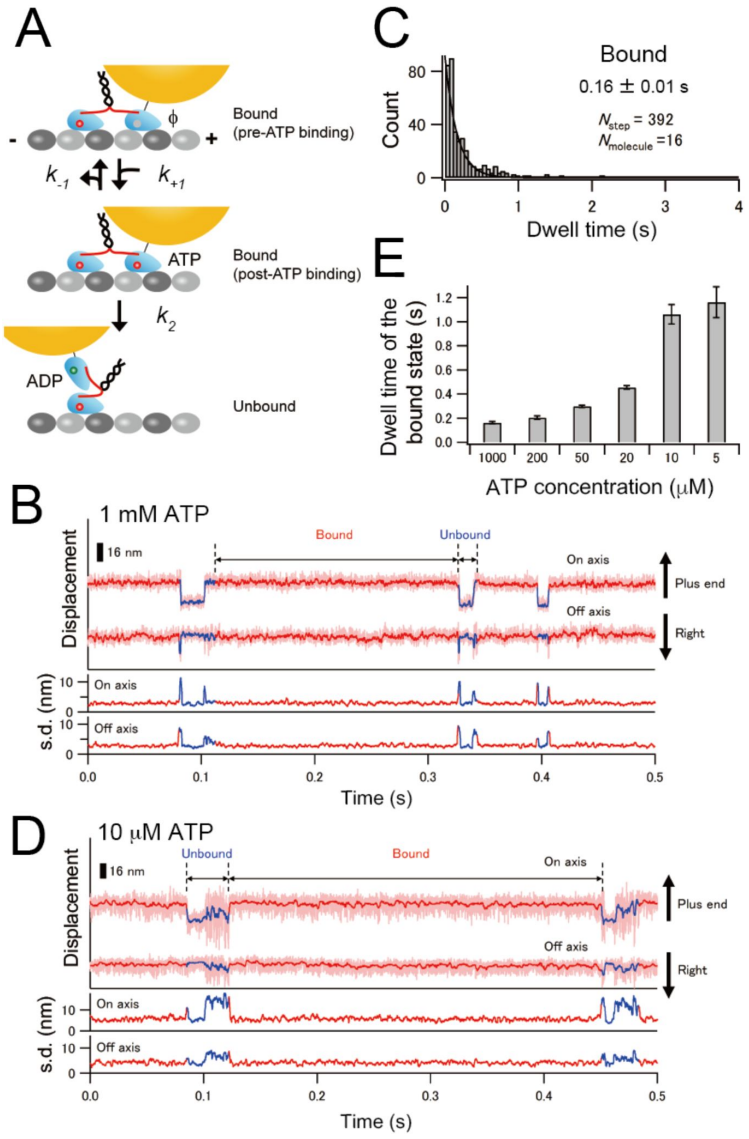

Figure 5.

Microtubule-detachment kinetics of the front WT head of E236A-WT heterodimer.

(**A**) A diagram illustrating the kinetic transitions for the detachment of the gold-labeled WT head of the E236A-WT heterodimer. Upon binding to the microtubule, the front head releases ADP, becoming a nucleotide-free state (indicated as Φ; pre-ATP binding). The detachment kinetics from this state can be described using the same scheme as the monomer (**Figure 1B**). (**B**) Typical trace for the centroid positions of the gold probe attached to the WT head of the E236A-WT heterodimer in the presence of 1 mM ATP (light red lines), toward the microtubule long axis (on axis) and perpendicular to the microtubule axis (off axis). Red and blue lines depict the median-filtered trace (with a window size of 51 frames) for the bound and unbound states, respectively. Lower panels display the standard deviation (s.d.) of on- and off-axis positions for each time frame t (calculated as [t – 20, t + 20]). (**C**) Histogram of the dwell time in the bound state. The solid line shows the fit with an exponential function. The number represents the average dwell time (± s.e.m.) determined from the fit. (**D**) Typical trace for the centroid positions of the gold probe attached to the WT head of E236A-WT heterodimer in the presence of 10 μM ATP. (**E**) Mean dwell times in the bound state under various ATP concentrations as determined from the fit of the histograms of the dwell times (**Figure 5–figure supplement 3**).

Figure supplement 1. Long-term trace of the gold-labeled E236A-WT heterodimer exhibiting very slow stepping motion.

Figure supplement 2. The unbound state of the gold-labeled WT head of the E236A-WT heterodimer.

Figure supplement 3. Distributions of the dwell time in the bound and unbound states of the leading WT head of E236A-WT heterodimer.

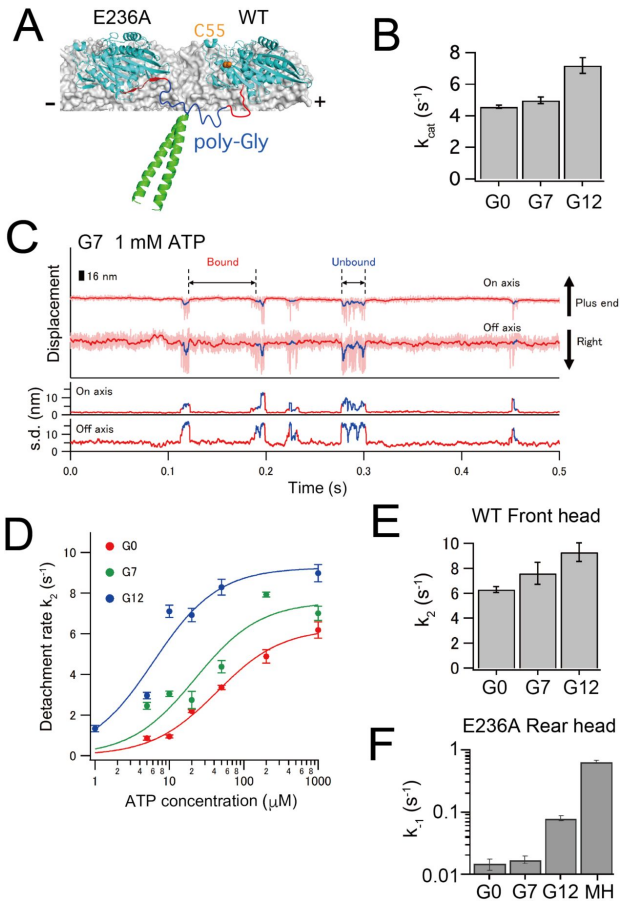

Figure 6.

Effect of the tension applied to the neck linker on the gating examined using the neck-linker extended E236A-WT heterodimer.

(**A**) Diagram showing the position of the poly-Gly residues (blue) inserted between the neck linker (red) and the neck coiled-coil (green). The Cys55 residue for gold-labeling is represented by an orange sphere. (**B**) k_{cat} for the microtubule-activated ATPase of E236A-WT heterodimers without (termed as G0) and with neck-linker extensions (G7 and G12) (**Figure 6–figure supplement 1**). (**C**) Typical trace for the centroid positions of the gold probe attached to the WT head of the E236A-WT heterodimer with a 7 poly-Gly insertion in the presence of 1 mM ATP. (**D**) The inverse of the mean dwell time in the bound state was plotted as a function of ATP concentration, as determined from the fit of the histograms of the dwell times (**Figure 6–figure supplement 2, 3**). Error bars represent s.e.m. The solid lines show the fit with the Michaelis-Menten equation. The fit parameters are k_{cat} (or k_2) = 6.3 ± 0.2 s^{-1} and K_m (ATP) = 43 ± 6 μM for G0, k_{cat} = 7.0 ± 0.5 s^{-1} and K_m (ATP) = 12 ± 3 μM for G7, and k_{cat} = 9.3 ± 0.7 s^{-1} and K_m (ATP) = 6.1 ± 2.1 μM for G12. The K_m (ATP) decreases as the insertion length increases. (**D**) The k_{cat} value, which represents the ATP-induced detachment rate of the front head k_2, obtained from the fit shown in panel **d**. The error bars represent s.e.m. (**F**) The ATP dissociation rates k_{-1} for the E236A rear head of the wild-type (G0), G7 and G12 E236A-WT heterodimer were determined using smFRET. The k_{-1} was calculated as the inverse of the mean dwell time for the high FRET state (see the typical trace and dwell time histograms for the G7 and G12 heterodimer in **Figure 6–figure supplement 5**). For comparison, data for the E236A monomer head (referred to as MH) is included from **Figure 2F**.

Figure supplement 1. Microtubule-activated ATPase rates of the E236A-WT heterodimer with and without neck-linker extension.

Figure supplement 2. Distributions of the dwell time in the bound and unbound states of the leading WT head of E236A-WT heterodimer with 7 poly-Gly insertion (G7).

Figure supplement 3. Distributions of the dwell time in the bound and unbound states of the leading WT head of E236A-WT heterodimer with 12 poly-Gly insertion (G12).

Figure supplement 4. Binding to the rear-tubulin binding site observed for the G12 E236-WT heterodimer.

Figure supplement 5. Single molecule FRET between donor-labeled E236A head of E236A-WT heterodimer with extended neck linker and acceptor-conjugated ATP.

detached from the rear-binding position much faster (19 ms at 1 mM ATP; **Figure 6–figure supplement 4**) than from the front-binding site (111 ms), indicating that the orientation of the neck linker has greater effect on the front head gating than the tension. These findings demonstrate that the detachment rate of the front head is not greatly affected by the amount of tension posed to the neck linker, at least within the range of 12 glycine insertions.

Next, we examined the effect of the tension posed to the neck linker on ATP off-rate k_{-1} of the rear E236A head of the E236A-WT heterodimer, by measuring smFRET between Cy3-labeled E236A head and Alexa-ATP. When compared to the heterodimer without neck linker extension (0.015 s^{-1}; **Figure 4E**), k_{-1} determined from the inverse of the mean dwell time of the high FRET state only modestly increased for G7 (0.018 s^{-1}) and increased by 5-fold for G12 (0.081 s^{-1}) (**Figure 6F** and **Figure 6–figure supplement 5**). The k_{-1} was further increased for monomeric E236A without neck linker constraint as described before (0.65 s^{-1}; **Figure 2F and 6F**). These results indicate that the ATP off-rate of the rear E236A head is significantly affected by the amount of the forward strain, especially when the neck linker was extended with more than 7 glycine insertions.

Discussion

To identify the chemical transition that is gated in the front and/or rear head, we measured ATP binding and microtubule detachment kinetics of kinesin's catalytic domain with neck linker constraints imposed by 1) disulfide crosslinking of the neck linker in monomeric kinesin in backward (rear head -like) and forward (front head -like) orientations, and 2) using the E236A-WT heterodimer to create a two-head microtubule-bound state with the mutant and WT heads occupying the rear and front positions respectively. As also described in the Results, these two experimental paradigms each have their unique caveats in terms of how faithfully they replicate a native moving kinesin dimer. We also used potentially perturbing measurement approaches that involve using fluorescently-labeled ATP or modifying cysteine-lite kinesin with fluorescent dyes or gold particles. However, the results from these two different experimental approaches and the variety of different measurements approaches all yielded consistent results, which are summarized below.

In the front head, backward orientation of the neck linker has little effect on ATP binding and dissociation rates, both when measured for a monomer crosslink (**Figure 2A, B**) and for the front head of a E236A-WT heterodimer (**Figure 4B, C, F**). These findings differ from a prevailing view that the ATP-binding step is gated in the front head (Rosenfeld et al., 2003; Klumpp et al., 2004; Guydosh and Block, 2006; Dogan et al., 2015). However, we found that the ATP-induced detachment rates from microtubule (k_2) were similarly reduced for both the front head crosslink (7.0 s^{-1}; **Figure 3A**) and the front WT head of the E236A/WT heterodimer (6.3 s^{-1}; **Figures 6D**), suggesting that a step subsequent to ATP binding is gated in the front head. These results are consistent with an inability of the front head to fully close its nucleotide pocket to promote ATP hydrolysis and Pi release (Benoit et al., 2023), as will be discussed later.

We also provide evidence for a rear-head gating mechanism that involves a tighter affinity for ATP (due to a decrease in reversible ATP-dissociation rate k_{-1}) without a change in microtubule affinity in the ATP-bound state. The K_d of ATP for the front head crosslink and the monomer without constraint are similar (~20 μM), and substantially higher than our estimated 4 nM K_d of ATP for the rear E236A head of the E236A-WT heterodimer. We note, however, that this K_d of ATP may somewhat underestimate the true value in wild-type kinesin for two reasons: first, the E236A mutation likely stabilizes the neck linker-docked, closed state more than in the rear head of the wild-type dimer (Rice et al., 1999), and second, the Alexa-ATP used to measure the ATP off-rate of E236A head showed ~10-fold smaller velocity compared to unmodified ATP, partly due to a slower ATP off-rate (Figure 2–figure supplement 3). While these caveats may diminish the observed 5000-fold difference in the K_d of ATP in native kinesin, these results nevertheless point to

large difference in ATP affinity between the front and rear heads. The difference in the ATP-affinity between the front and rear heads can explain previous experimental results supporting the front-head gating mechanism (Uemura and Ishiwata, 2003; Rosenfeld et al., 2003; Klumpp et al., 2004; Guydosh and Block, 2006; Dogan et al., 2015), although our direct kinetic measurements show that this difference is manifest through in a stronger affinity for ATP in the rear head rather than a weaker affinity in the front head. While the neck linker position of the rear head increases the affinity of bound ATP, it does not significantly accelerate k_2, which includes the ATP hydrolysis and Pi release steps in the chemical cycle.

Kinetic gating aids head-head coordination but does not prevent progression through the ATPase cycle

Our results show that the front head gate slows down but does not block its ATPase cycle. The ATP-induced microtubule detachment rate k_2 of the front head is 6-7 s^{-1} (7.0 s^{-1} for the front head monomer crosslink and 6.3 s^{-1} for the front head of E236A-WT heterodimer) which is similar to its overall ATPase rate (4.6 s^{-1}). These rate constants are sufficiently low to keep the catalytic cycles of two heads largely out of phase, since the detachment rate of the rear head of wild-type dimer (inverse of the dwell time from two-head-bound state to one-head-bound state during processive movement) is ~100 s^{-1} (Isojima et al., 2016). The observed detachment of the front head of E236A-WT heterodimer is likely caused by ATP hydrolysis of the front head, because 1) ATP turnover rate of this heterodimer was similar to the k_2 value, and 2) the dwell time of the bound state of the front head on microtubule was dependent on the ATP concentration. These results suggest that the kinesin's head can slowly hydrolyze ATP and detach from microtubule without the aid of neck-linker docking. This idea can explain how kinesin dimer takes repetitive back steps under large hindering loads. Carter and Cross (2005) showed that kinesin takes 8-nm backward steps at supra-stall forces (>7 pN) exerted using an optical trap, and that the stepping rate was dependent on the ATP concentration (~0.3 steps/s and ~1 step/s at 1 mM and 10 μM ATP conditions, respectively), which are comparable to the dwell times that we found for the microtubule-bound state of the front head of E236A-WT heterodimer (0.16 s and 1.1 s at 1 mM and 10 μM ATP, respectively; Figure 5–figure supplement 3). These results suggest that the back steps are likely caused by the neck-linker docking-independent slow ATP catalysis of the front head followed by its dissociation from the microtubule in an ADP-bound state.

A kinetic and structural model for kinesin gating

The difference in the ATP binding affinity between the front (low affinity) and rear (high affinity) heads suggests a structural difference in their nucleotide binding pockets. Indeed, the high ATP affinity state of the neck linker -docked rear head is consistent with a "closed" nucleotide pocket observed in crystal and cryo-EM structures of kinesin-1 bound to tubulin and complexed with a non-hydrolyzable ATP analog in kinesin's active site (Shang et al., 2005; Gigant et al., 2013). Moreover, a recent high-resolution cryo-EM image of the microtubule-bound KIF14 dimer showed that while they could observe nucleotide in the active site of the front head, the structure of the pocket was more "open" and similar to that of a nucleotide-free head (Shang et al., 2014; Cao et al., 2014; Benoit et al., 2021). Since the switch I and II loops that are involved in hydrolysis reaction are positioned away from the ψ-phosphate in the opened nucleotide pocket, the open state is incompatible with ATP hydrolysis, while the closed state is competent in ATP hydrolysis (Kull and Endow, 2002; Parke et al., 2010) (Figure 7–figure supplement 1B). Thus, these structural features are consistent with our kinetics results.

These findings suggest that the isomerization from the open to closed conformational state, rather than the chemical transition, is gated by the neck linker constraint (Figure 7–figure supplement 2). This aligns with our structural modeling of kinesin dimer in the two-head-bound state (Makino et al., 2024), which showed that conformational transitions are suppressed for both the front head (from open to closed state) and the rear head (from closed to open state), as these changes would cause an intolerable increase in tension on the disordered neck linker region

(**Figure 7**). We demonstrated, using the loose C47/C335 backward crosslink of the neck linker, that neck linker docking is responsible for opening the gate (i.e., the open to closed transition) (**Figure 3A-D**). The C47/C335 crosslink forms a short 7-amino acid flexible loop, which is insufficient for the formation of two β-sheets (residues 326-334) (**Figure 3–figure supplement 3**). However, it allows the conformational transition of the initial segment of the neck linker (residues 323-325); K323 and T324 residues form an α-helix extending the C-terminus of α6, while the I325 residue plays a particularly important role in docking onto the hydrophobic pocket exposed on the closed head. Given that the hydrophobic pocket is positioned forward from the neck linker's base (**Figure 7–figure supplement 1A**), the docking of the I325 side chain is suppressed in the front head, as it would cause an intolerable increase in tension (entropy decrease) on the disordered neck linker (Makino et al., 2024), thus maintaining the open state. The neck linker extension had a smaller effect on front-head gating (**Figure 6E**), likely because a stable interaction between the I325 side chain and the hydrophobic pocket is necessary to maintain the closed state until ATP hydrolysis completes. In contrast, the neck linker extension had a larger effect on the rear head's ATP affinity (**Figure 6F**). This is probably because the rear head can occasionally transition back to an open state (followed by reversible ATP release) without tension on the neck linker (**Figure 2D**; Rice et al., 2003). Thus, forward strain plays a crucial role in aiding I325 residue docking and stabilizing the closed state.

In summary, our findings, together with structural data discussed above, are consistent with an asynchronous sequence of events in the front and rear kinesin heads that help to coordinate their chemomechanical cycles to ensure their continuous stepping along the microtubule (**Figure 7**). In the rear head, ATP binding is followed rapidly by an isomerization step that closes the nucleotide pocket, decreasing the rate of nucleotide dissociation and facilitating ATP hydrolysis. This conformational change is facilitated by docking of the neck linker in its forward orientation (Benoit et al., 2003). In the front head, in contrast, the backward conformation of neck linker favors an open nucleotide pocket, which helps to prevent the microtubule-bound front head from proceeding with ATP hydrolysis before the rear head detaches. Once the rear head detaches, the front head "gate" is relieved, allowing the neck linker to dock and its nucleotide pocket to close. This asynchrony in the timing of ATP hydrolysis minimizes the likelihood of both heads simultaneously entering an ADP-state and dissociating from microtubule. Recent cryo-EM studies and modeling of the kinesin dimer under various nucleotide states support the proposal that the open-closed conformational transition is gated by the neck linker strain; however, direct evidence for this conformational transition in the context of a processively moving kinesin dimer would help to further substantiate this model.

Materials and methods

DNA cloning and protein purification

We used a 339 amino-acid "cysteine-light" mutant or a 349 amino-acid wild-type human kinesin-1 monomer as a template for mutagenesis. Cysteines and/or a E236A point-mutation were introduced by PCR cloning involving QuikChange mutagenesis (Stratagene) (Tomishige and Vale, 2000). For heterodimer, mutations were introduced into one of the two polypeptide chains of the cysteine-light kinesin-1 heterodimer with 490 amino-acids (Tomishige et al., 2006; Isojima et al., 2016). For single molecule fluorescent observation of monomers, GFP (P64L/S65T variant) was fused at the C-terminal of constructs. All the constructs were verified by DNA sequencing. Kinesin proteins were expressed and purified as described previously (Tomishige and Vale, 2000; Tomishige et al., 2006) except that for monomeric kinesins, Ni-NTA chromatography was followed by dialysis against 25 mM PIPES (pH 7.0), 100 mM NaCl, 2 mM $MgCl_2$ and 100 μM ATP for 3 h at 4°C. EGTA in the buffer was removed. For steady state ATPase assays and single molecule observations, proteins were further purified with microtubule-affinity purification (Tomishige et al., 2006). DTT and EGTA were removed from the solutions. Tubulin was purified and

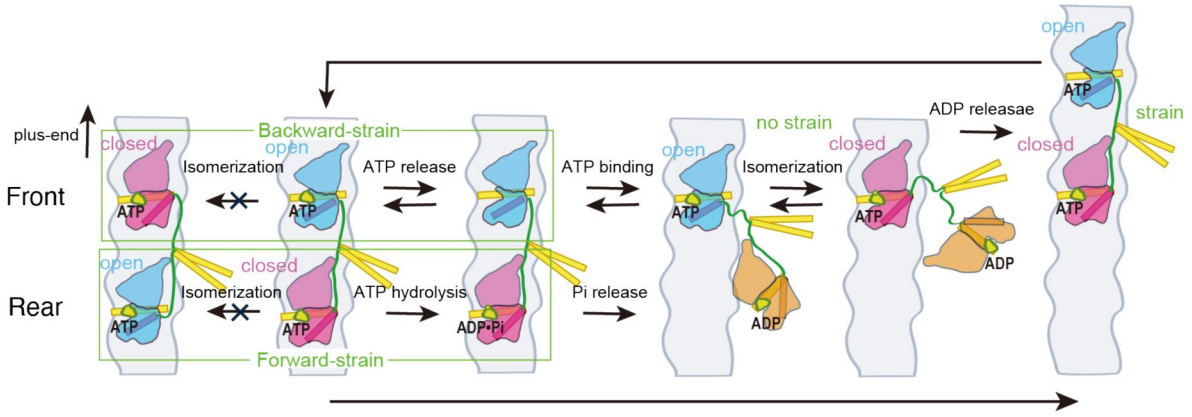

Figure 7.

Model to explain how the tension exerted by the stretched neck linker in dimeric kinesin coordinates the microtubule detachment of the two heads.

This model is based on the proposal that the transition between ATP-bound open and closed conformations of the head is regulated by the neck linker strain (Figure 7–figure supplement 2). The open and closed conformational states of the head are indicated in blue and red, respectively, with the α6 helix, which connects to the neck linker, highlighted as a rod. The microtubule-detached ADP-bound state is shown in orange. The neck linker is depicted in green, while the α4 helix, which directly interacts with the microtubule, and the neck coiled-coil are shown in yellow. In the two-head-bound state, the front head remains in the open state because the backward strain prevents it from transitioning to the closed state. In this state, ATP can weakly bind to the nucleotide-pocket but often dissociates. Conversely, the rear head is stabilized in the closed state because the transition to the open state is suppressed by the forward strain. ATP is tightly bound to the closed nucleotide-pocket, causing the rear head to hydrolyze ATP and detach from the microtubule before the front head does. In the one-head-bound state, the microtubule-bound head can transition between the open and closed states. However, once the tethered head binds preferentially to the forward tubulin-binding site, the strain built up between the two microtubule-bound heads stabilizes the rear head in the closed conformation and the front head in the open conformation.

Figure supplement 1. Structural difference between the open and closed conformational states of the kinesin head.

Figure supplement 2. Schematic model showing that the open-closed conformational transition (isomerization) is gated by the neck linker strain.

polymerized as described previously (Woehlke et al., 1997). Protein concentrations were determined by Bradford assays using BSA as a standard. For fluorescent labeling (smFRET or mant-ATP binding measurement of heterodimer), dialyzed kinesin was reacted with Cy3-maleimide (Cytiva), Cy5-maleimide (Cytiva), ATTO488-maleimide (ATTO-TEC) or Alexa488-maleimide (Thermo Fisher). The labeled protein was further purified through microtubule affinity purification as described (Yildiz et al., 2004; Tomishige et al., 2006).

Chemical cross-linking

Disulfide cross-link was formed by oxidation using copper and phenanthroline (Kobashi, 1968; Kaan et al., 2011). Reactions were carried out by addition of 10 μM $CuCl_2$ and 20 μM o-phenanthroline to 4 μM kinesin heads in 25 mM PIPES (pH 6.8) plus 2 mM $MgCl_2$ and incubation on ice for 3 h. The reactions were quenched by addition of 1 mM EGTA. Control reactions were carried out in parallel by adding 10 mM DTT. Disulfide cross-linking was verified using non-reducing SDS-PAGE with AMS (4'-acetamido-4'-maleimidylstilbene-2,2'-disulfonic acid, 6508; Setareh Biotech) which react with reduced cysteine residues causing band-shift on SDS-PAGE (Denoncin et al., 2013). Post cross-linking reaction of kinesin (after addition of EGTA) was denatured by addition of 10% trichloroacetic acid (TCA) and incubation for 30 min at 4°C. 100 μl of denatured kinesin solution was centrifuged (100k rpm, for 5 min) and pellet was carefully washed with 50 mM Tris-HCl (pH 7.5) plus 10 mM EDTA to remove DTT or copper. The pellet was then resuspended in 30 μl of solution containing 50 mM Tris-HCl (pH 7.5), 10 mM EDTA, 0.1% SDS, 20 mM AMS. The sample was incubated over night at room temperature under shaking. Addition of SDS sample buffer without reducing reagents was followed by SDS-PAGE (8.5% polyacrylamide) and CBB staining. Ratio of reduced and oxidized molecules was quantified using ImageJ.

Steady state ATPase assay

Microtubule-stimulated ATPase activity was measured using spectrometer (V550; JACSO) with a coupled enzymatic assay as described previously (Woehlke et al., 1997). The ATPase assays were performed in BRB12 buffer (12 mM PIPES (pH 6.8), 2 mM $MgCl_2$, 1 mM EGTA) containing 1 mM ATP, 20 μM taxol, 0.1 mg/ml casein and coupled NADH oxidation system (0.2 mM NADH, 5 mM phospho(enol)pyruvate, 10 μg/ml of pyrvate kinase, and 10 μg/ml of lactate dehydrogenase). 1 mM DTT was also added when measuring reducing conditions. The assays were started with 10 nM kinesin and varying concentrations of microtubules at 22°C.

Pre-steady state kinetics measurements

All stopped flow experiments were performed at 25°C in BRB25 buffer (25 mM PIPES (pH 6.8), 2 mM $MgCl_2$, 1 mM EGTA) using a KinTek Stopped flow system (SF2004; Kintek Corp., State College, PA) with a Xenon lamp. Mant-nucleotide fluorescence measurements were performed using an extension wavelength of 280 nm and fluorescence emission was monitored using a 445/40 band pass filter (D445/40M; Chroma Tec). 5-10 fluorescent traces were averaged for each experimental condition. Turbidity measurements were performed at 340 nm and 15-20 turbidity traces were averaged. Averaged stopped flow traces were fit to single exponential function,

$$y = A\ exp(-k_{obs}t) + C \qquad \text{(Eq. 1)}$$

or a burst equation,

$$y = A\ exp(-k_{obs}t) + k_{ss}t + C \qquad \text{(Eq. 2)}$$

where k_{obs} is the rate constant of the initial exponential phase, k_{ss} is the rate constant of the linear phase, A is the amplitude of exponential phase and C is the constant term.

Mant-ATP binding kinetics

Microtubule-kinesin complex was prepared by incubation of 3.2 μM post cross-linking kinesin with 4 μM microtubule and 20 μM taxol in BRB25 buffer at room temperature for 10 min. Microtubule-C222/C334 kinesin complex was prepared by following procedure. 3.2 μM of reduced/oxidized C222/C334 kinesin was incubated with 4 μM microtubules, 20 μM taxol and 5 U/ml apyrase at room temperature for 1 h, followed by a centrifugation (80k rpm, 10 min) on 20% sucrose cushion. For Alexa488-labeled heterodimer, 5 μM of heterodimer kinesin was incubated with 25 μM microtubules in the presence of 1 mM ATP at room temperature for 10 min, followed by a centrigugation (80k rpm, 10 min) on 60% glycerol cushion. The pellet was resuspended in initial volume of BRB25 plus 20 μM taxol. The concentration of the heterodimer-microtubule complex was estimated using the extinction coefficient of Alexa488 dye (73,000 $cm^{-1}M^{-1}$) and was adjusted to approximately 1 μM after mixing. The microtubule-kinesin complex was then rapidly mixed with increasing concentrations of mant-ATP (M12417; Invitrogen) or mant-dATP (3'-O-(N-Methyl-anthraniloyl)-2'-deoxyadenosine-5'-triphosphate; Jena Bioscience). Fluorescence data of mantATP binding were fit to single exponential (Eq. 1). Values of k_{obs} were plotted against nucleotide concentration and fit to linear function,

$$k_{obs} = k_{+1}[\text{mantATP}] + k_{-1} \qquad \text{(Eq. 3)}$$

where k_{+1} is the second-order rate constant for nucleotide binding and k_{-1} is the rate constant for nucleotide dissociation from the motor.

Microtubule dissociation kinetics

Microtubule-kinesin complex was prepared by incubation of 3.2 μM post cross-linking kinesin with 4 μM microtubule, 20 μM taxol and 0.1 U/ml apyrase in BRB25 buffer at room temperature for 10 min. 150 mM KCl was then added into kinesin solution. The change in turbidity was monitored after rapid mixing of microtubule-kinesin complex with ATP (1 mM post mixing) plus 150 mM KCl. Turbidity traces were fit to burst equation (Eq. 2) to determine microtubule dissociation rate.

Single molecule fluorescence observation of GFP-labeled kinesin

Binding/detachment of individual GFP-fused kinesin on axonemes (purified from sea urchin sperm flagella) were observed in a custom-build prism-type laser-illuminated total-internal-reflection microscope as described (Tomishige and Vale, 2000). Assay chamber constructed between a quartz slide and a coverslip was first filled with axonemes diluted in BRB12 for 3min, followed by a washing with 1mg/ml casein in BRB12 for 3 min. The chamber was then filled with the assay solution contained GFP-kinesin (200 pM for WT, C47/C328 and C47/C335, 500 pM for C222/C334 and C4/C330), 1 mM ATP, 100 mM KCl and oxygen scavenging system (4.5 mg/ml glucose, 50 U/ml catalase, 50 U/ml glucose-oxidase) and sealed. 70 mM 2-mercaptoethanol was added in the assay solution when observing in reducing condition. GFP molecules were exited at 488 nm and fluorescence was recorded at 10 ms temporal resolution. Distributions of dwell time on axonemes were obtained from kymographs. Fluorescent spots dwelled more than two frames were used for analysis. Detachment rates were determined by single exponential fitting of the dwell histograms.

Flow-cell chamber preparation for single molecule FRET

For the wild-type monomeric kinesin, flow-cell chamber was constructed between poly-L-lysine-coated quartz slide and cover slip. The chamber was first filled with microtubule in BRB12 buffer containing 20 μM taxol for 5 min. Then, BRB12 buffer containing 20 μM taxol and 1 mg/ml casein was infused and incubated for 2 min followed by washing with BRB12 buffer containing 20 μM taxol. The chamber was finally filled with observation buffer containing an ATP regenerating system (10 μg/ml creatin kinase, 2 mM creatin phosphate), an oxygen scavenging system (2.5 mM protocatechuic acid (PCA), 1 unit/ml protocatechuate-3,4-dioxygenase (PCD) (P8279-25UN; Sigma),

2 mM Trolox) (Aitken et al., 2008), 150 mM KCl, 20 μM taxol, 500 nM Alexa Fluor 647 ATP (A22362; Invitrogen) and 100 pM kinesin in BRB12 buffer. All procedures were carried out at room temperature.

For the other constructs (E236A monomer, E236A-WT heterodimer), flow-cell chamber was constructed between quartz slide pre-cleaned with 0.1 M KOH and cover slip, separated by ~50 μm thickness. The cell was first filled with Protein A (Sigma P6031-1MG) solution (20 μl, 50 μg/ml) in BRB12 buffer (12 mM PIPES (pH 6.8), 2 mM $MgCl_2$, 1 mM EGTA) for 2 min. After washing unbound protein with 40 μl of BRB12 buffer, 20 μl of 20 μg/ml anti-α-tubulin antibody (Sigma T6199) solution in BRB12 buffer was infused for 5 min. Then unbound antibody was washed out with 40 μl of BRB12 buffer containing 20 μM taxol. Then, 40 μl of microtubule suspension in BRB12 buffer containing 20 μM taxol was infused and incubated for 2 min. Then, 40 μl of BRB12 buffer containing 20 μM taxol and 1 mg/ml casein was infused and incubated for 2 min. After washing with 40 μl of BRB12 buffer containing 20 μM taxol, the chamber was finally filled with observation buffer containing an ATP regenerating system (10 μg/ml creatin kinase, 2 mM creatin phosphate), an oxygen scavenging system (4.5 mg/ml glucose, 50 unit/ml glucose-oxidase, 50 unit/ml catalase, 0.5% 2-mercaptoethanol), 20 μM taxol, 200 nM Alexa Fluor 647 ATP (A22362; Invitrogen) and 100 pM kinesin in BRB12 buffer. All procedures were carried out at room temperature.

Single molecule FRET observation

Single molecule observation of fluorescently labeled kinesin was done under a prism-type total internal reflection fluorescence microscopy (Mori et al., 2007). We used ATTO 488 (WT monomer) and Cy3 (others) as a donor fluorophore. ATTO 488 was excited with 488 nm diode laser (Cyan-75-TA-FE; Spectra-Physics Inc.) and Cy3 was excited with 515 nm diode laser (EXLSR-515-50-CDTF-E, Spectra-Physics Inc.). Fluorescent signals were collected through objective lens and a specific filter for cutting of the excitation light and projected on a cooled EMCCD camera. For smFRET observations, fluorescent signal was separated using dichroic mirror and donor and acceptor fluorescence were simultaneously observed. Position of microtubule was identified based on the fluorescence from the labeled kinesin. When more than 5 fluorescent spots of donor fluorophore lied on a straight line, we assumed that these spots were on the microtubule. FRET data were collected at 10 ms and 200 ms exposure times for wild-type monomer and for E236A monomer and E236A-WT heterodimer, respectively, at 22 °C. We identified ATP binding to the kinesin head when the FRET efficiency exceeded a threshold of 0.5.

Gold labeling of kinesin

Purified kinesin was biotinylated, and biotinylated kinesin was bound to microtubules in the presence of AMP-PNP as described previously (Isojima et al., 2016). Microtubule-bound kinesin was then collected by centrifugation (230,000*g* for 10 min) and was immersed in streptavidin solution containing 12 mM PIPES (pH6.8), 2 mM $MgCl_2$, 1 mM EGTA, 20 μM taxol and 2.5 mg/ml streptavidin (191-12851; Wako Pure Chemical Industries) and incubated 20 min at room temperature. Microtubule-bound streptavidin-modified kinesin was collected by centrifugation (230,000g for 10 min) and released from microtubules as described previously. Biotin-coated gold nanoparticles were prepared as previously described (Isojima et al., 2016), except that streptavidin was not added to the gold. Just before observation, streptavidin-modified kinesin and biotin-coated gold nanoparticles were mixed at a 1:1 molecule/particle ratio.

Total internal reflection dark-field microscopy

A flow cell was constructed, and microtubules were attached on the glass surface by using protein A and anti-α-tubulin antibody as described previously (Isojima et al., 2016). The cell was then infused with 40 μl of BRB 12 buffer (12 mM PIPES (pH 6.8), 2 mM EGTA and 1 mM $MgCl_2$) containing 20 μM taxol and 1 mg/ml casein for 2 min. The cell was infused with BRB12 buffer containing 3 nM gold-labeled kinesin for 5 min, and unbound kinesins and gold nanoparticles

were removed by washing with 60 µl of the BRB12 buffer containing 20 µM taxol. Finally, the flow cell was infused with 40 µl of the observation buffer (BRB12 buffer containing 70 mM β-mercaptoethanol, 10 µg/ml creatine kinase, 2 mM creatine phosphate, 20 mM KCl and 1-1000 µM ATP), sealed with nail polish and used for observation. All procedures were carried out at room temperature. The gold-labeled kinesin was observed using a total internal reflection dark-field microscope as described previously (Isojima et al., 2016) and the scattering images were recorded with a high-speed CMOS camera (FASTCAM Mini AX100; Photron) at a frame rate of 20,000 fps (50 µs temporal resolution). Observations were carried out at 24-26°C.

Data analysis for the dark-field observations

The coordinates of gold nanoparticles were determined as described previously (Isojima et al., 2016). The orientations of the microtubule 'on axis' (orientation parallel to the microtubule long axis) and 'off axis' (orientation perpendicular to the microtubule long axis) were then determined from the aligned gold-labeled kinesin along the microtubule and adjusted to X and Y coordinates as described previously. The 'bound' and 'unbound' states of gold-labeled kinesin heads were determined as follows: two-dimensional standard deviation (s.d.) of the trajectory for each time frame t was calculated as [t - 20, t + 20] and the median µ and s.d. σ of the s.d. of the trajectory was determined by fitting the histogram of the s.d. with a Gaussian function. Transitions from the bound to unbound state were detected when the s.d. was higher than µ+4σ in 10 consecutive frames and transition from the unbound to bound state were detected when the s.d. was lower than µ+4σ in 10 consecutive frames. The accurate frame of the transition was determined by fitting the on- and off-axis trajectory near the transition with two state step function. In the case of G0 construct, if two unbound states were closer than 50 ms and on-axis average of the bound state between these unbound states was separated from the other bound states, these unbound states and bound state were determined as unbound state 1-3 (Figure 4–figure supplement 2). The rate constants of each state were determined by fitting the histogram of the dwell time with single exponential functions.

Acknowledgements

We thank M. Nakajima and Y. Sakai for support with cloning. M.T. was supported by MEXT KAKENHI Grant Number 17H03661 and by JSPS KAKENHI Grant Numbers JP20H05542, JP22H04850.

Additional information

Author contributions

Yamato Niitani, Conceptualization, Investigation, Formal analysis, Software, Methodology, Visualization; Kohei Matsuzaki, Investigation, Formal analysis, Software, Methodology, Visualization; Erik Jonsson, Investigation, Formal analysis, Methodology; Ronald Vale, Methodology, Supervision, Funding acquisition, Writing – review and editing; Michio Tomishige, Conceptualization, Methodology, Supervision, Funding acquisition, Writing – original draft, Project administration, Writing - review and editing

Additional files

Supplemental Figures

References

Aitken C. E., Marshall R. A., Puglisi J. D (2008) **An oxygen scavenging system for improvement of dye stability in single-molecule fluorescence experiments** *Biophys. J* **94**:1826–1835

Andreasson J. O. L., et al. (2015) **Examining kinesin processivity within a general gating framework** *eLife* **4**:e07403

Asbury C. L., Fehr A. N., Block S. M (2003) **Kinesin moves by an asymmetric hand-over-hand mechanism** *Science* **302**:2130–2134

Asenjo A. B., Krohn N., Sosa H (2003) **Configuration of the two kinesin motor domains during ATP hydrolysis. Nature Struct** *Biol* **10**:836–842

Auerbach S. D., Johnson K. A (2005a) **Alternating site ATPase pathway of rat conventional kinesin** *J. Biol. Chem* **280**:37048–37060

Auerbach S. D., Johnson K. A (2005b) **Kinetic effects of kinesin switch I and switch II mutants** *J. Biol. Chem* **280**:37061–37068

Benoit M. P. M. H., et al. (2021) **Structural basis of mechano-chemical coupling by the mitotic kinesin KIF14** *Nat. Commun* **12**:3637

Benoit M. P. M. H., Hunter B., Allingham J. S., Sosa H (2023) **New insights into the mechanochemical coupling mechanism of kinesin-microtubule complexes from their high-resolution structures** *Biochem. Soc. Trans* **51**:1505–1520

Block S. M (2007) **Kinesin motor mechanics: binding, stepping, tracking, gating, and limping** *Biophys. J* **92**:2986–2995

Cao L., et al. (2014) **The structure of apo-kinesin bound to tubulin links the nucleotide cycle to movement** *Nat. Commun* **5**:5364

Carter N. J., Cross R. A (2005) **Mechanics of the kinesin step** *Nature* **435**:308–312

Cochran J. C (2015) **Kinesin motor enzymology: chemistry, structure, and physics of nanoscale molecular machines** *Biophys. Rev* **7**:269–299

Crevel I. M.-T., et al. (2004) **What kinesin does at roadblocks: the coordination mechanism for molecular walking** *EMBO J* **23**:23–32

Cross R. A (2004) **The kinetic mechanism of kinesin** *Trends Biochem. Sci* **29**:301–309

Denoncin K., Nicolaes V., Cho S.-H., Leverrier P., Collet J.-F (2013) **Protein disulfide bond formation in the periplasm: determination of the in vivo redox state of cysteine residues** *Methods Mol. Biol* **966**:325–336

Dogan M. Y., Can S., Cleart F. B., Purde V., Yildiz A (2015) **Kinesin's front head is gated by the backward orientation of its neck linker** *Cell Rep* **10**:1967–1973

Gennerich A., Vale R. D (2009) **Walking the walk: how kinesin and dynein coordinate their steps** *Curr. Opin. Cell Biol* **21**:59–67

Gigant B., et al. (2013) **Structure of a kinesin–tubulin complex and implications for kinesin motility** *Nat. Struct. Mol. Biol* **20**:1001–1007

Gilbert S. P., Johnson K. A (1994) **Pre-steady-state kinetics of the microtubule-kinesin ATPase** *Biochemistry* **33**:1951–1960

Gilbert S. P., Moyer M. L., Johnson K. A (1998) **Alternating site mechanism of the kinesin ATPase** *Biochemistry* **37**:792–799

Guydosh N. R., Block S. M (2006) **Backsteps induced by nucleotide analogs suggest the front head of kinesin is gated by strain** *Proc. Natl. Acad. Sci. USA* **103**:8054–8059

Hackney D. D (1994) **Evidence for alternating head catalysis by kinesin during microtubule-stimulated ATP hydrolysis** *Proc. Natl. Acad. Sci. USA* **91**:6865–6869

Hackney D. D., Stock M. F., Moore J., Patterson R. A (2003) **Modulation of kinesin half-site ADP release and kinetic processivity by a spacer between the head groups** *Biochemistry* **42**:12011–12018

Hancock W. O., Howard J (1999) **Kinesin's processivity results from mechanical and chemical coordination between the ATP hydrolysis cycles of the two motor domains** *Proc. Natl. Acad. Sci. USA* **96**:13147–13152

Hariharan V., Hancock W. O (2009) **Insights into the mechanical properties of the kinesin neck linker domain from sequence analysis and molecular dynamics dimulations** *Cel Mol Bioeng* **2**:177–189

Hwang W., Lang M. J., Karplus M (2008) **Force generation in kinesin hinges on cover-neck bundle formation** *Structure* **16**:62–71

Hyeon C., Onuchic J. N (2007) **Internal strain regulates the nucleotide binding site of the kinesin leading head** *Proc. Natl. Acad. Sci. USA* **104**:2175–2180

Isojima H., Iino R., Niitani Y., Noji H., Tomishige M (2016) **Direct observation of intermediate states during the stepping motion of kinesin-1. Nature Chem** *Biol* **12**:290–297

Jiang W., Hackney D. D (1997) **Monomeric kinesin head domains hydrolyze multiple ATP molecules before release from a microtubule** *J. Biol. Chem* **272**:5616–5621

Kaan H. Y. K., Hackney D. D., Kozielski F (2011) **The structure of the kinesin-1 motor-tail complex reveals the mechanism of autoinhibition** *Science* **333**:883–885

Kaseda K., Higuchi H., Hirose K (2003) **Alternate fast and slow stepping of a heterodimeric kinesin molecule** *Nature Cell Biol* **5**:1079–1082

Klumpp L. M., Hoenger A., Gilbert S. P. (2004) **Kinesin's second step** *Proc. Natl. Acad. Sci. USA* **101**:3444–3449

Khalil A. S., et al. (2008) **Kinesin's cover-neck bundle folds forward to generate force** *Proc. Natl. Acad. Sci. USA* **105**:19247–19252

Kobashi K (1968) **Catalytic oxidation of sulfhydryl groups by o-phenanthroline copper complex** *Biochim. Biophys. Acta* **158**:239–245

Kull F. J., Endow S. A. (2002) **Kinesin: switch I & II and the motor mechanism** *J. Cell Sci* **115**:15–23

Liu D., Liu X., Shang Z., Sindelar C. V (2017) **Structural basis of cooperativity in kinesin revealed by 3D reconstruction of a two-head-bound state on microtubule** *eLife* **6**:e24490

Ma Y.-Z., Taylor E. W (1997a) **Kinetic mechanism of a monomeric kinesin construct** *J. Biol. Chem* **272**:717–723

Ma Y.-Z., Taylor E. W (1997b) **Interacting head mechanism of microtubule-kinesin ATPase** *J. Biol. Chem* **272**:724–730

Makino T., et al. (2024) **Tension-induced suppression of allosteric conformational changes explains coordinated stepping of kinesin-1** *bioRxiv*

Mori T., Vale R. D., Tomishige M (2007) **How kinesin waits between steps** *Nature* **450**:750–754

Moyer M. L., Gilbert S. P., Johnson K. A (1998) **Pathway of ATP hydrolysis by monomeric and dimeric kinesin** *Biochemistry* **37**:800–813

Parke C. L., Wojcik E. J., Kim S., Worthylake D. K (2010) **ATP hydrolysis in Eg5 kinesin involves a catalytic two-water mechanism** *J. Biol. Chem* **285**:5859–5867

Rice S., et al. (1999) **A structural change in the kinesin motor protein that drives motility** *Nature* **402**:778–784

Rice S., et al. (2003) **Thermodynamic properties of the kinesin neck-region docking to the catalytic core** *Biophys. J* **84**:1844–1854

Rosenfeld S. S., et al. (2003) **Stepping and stretching: how kinesin uses internal strain to walk processivity** *J. Biol. Chem* **278**:18550–18556

Schief W. R., Clark R. H., Crevenna A. H., Howard J (2004) **Inhibition of kinesin motility by ADP and phosphate supports a hand-over-hand mechanism** *Proc. Natl. Acad. Sci. USA* **101**:1183–1188

Shang Z., et al. (2014) **High-resolution structures of kinesin on microtubules provide a basis for nucleotide-gated force-generation** *eLife* **3**:e04686

Shastry S., Hancock W. O (2010) **Neck linker length determines the degree of processivity in kinesin-1 and kinesin-2 motors** *Curr. Biol* **20**:939–943

Sindelar C. V (2011) **A seesaw model for intermolecular gating in the kinesin motor protein** *Biophys. Rev* **3**:85–100

Skiniotis G., et al. (2003) **Nucleotide-induced conformations in the neck region of dimeric kinesin** *EMBO J* **22**:1518–1528

Tomishige M., Vale R. D (2000) **Controlling kinesin by reversible disulfide cross-linking: identifying the motility-producing conformational change** *J. Cell Biol* **151**:1081–1092

Tomishige M., Stuurman N., Vale R. D (2006) **Single-molecule observations of neck linker conformational changes in the kinesin motor protein. Nature Struct** *Mol. Biol* **13**:887–894

Uemura S., et al. (2002) **Kinesin-microtubule binding depends on both nucleotide state and loading direction** *Proc. Natl. Acad. Sci. USA* **99**:5977–5981

Uemura S., Ishiwata S (2003) **Loading direction regulates the affinity of ADP for kinesin. Nature Struct** *Biol* **10**:308–311

Vale R. D., Milligan R. A (2000) **The way things move: looking under the hood of molecular motor proteins** *Science* **288**:88–95

Valentine M. T., Gilbert S. P (2007) **To step or not to step? How biochemistry and mechanics influence processivity in kinesin and Eg5** *Curr. Opin. Cell Biol* **19**:75–81

Wolff J. O., et al. (2023) **MINFLUX dissects the unimpeded walking of kinesin-1** *Science* **379**:1004–1010

Yildiz A., Tomishige M., Vale R. D., Selvin P. R. (2004) **Kinesin walks hand-over-hand** *Science* **303**:676–678

Yildiz A., Tomishige M., Gennerich A., Vale R. D (2008) **Intramolecular strain coordinates kinesin stepping behavior along microtubules** *Cell* **134**:1030–1041

Author information

Yamato Niitani[†]
Department of Applied Physics, School of Engineering, The University of Tokyo, Tokyo, Japan

[†]These authors contributed equally to this work.

Kohei Matsuzaki[†]
Department of Applied Physics, School of Engineering, The University of Tokyo, Tokyo, Japan, Department of Physical Sciences, College of Science and Engineering, Aoyama Gakuin University, Sagamihara, Japan

[†]These authors contributed equally to this work.

Erik Jonsson
Howard Hughes Medical Institute and Department of Cellular and Molecular Pharmacology, University of California, San Francisco, San Francisco, United States

Ronald D Vale
Howard Hughes Medical Institute and Department of Cellular and Molecular Pharmacology, University of California, San Francisco, San Francisco, United States

Michio Tomishige
Department of Applied Physics, School of Engineering, The University of Tokyo, Tokyo, Japan, Department of Physical Sciences, College of Science and Engineering, Aoyama Gakuin University, Sagamihara, Japan

For correspondence: tomishige@phys.aoyama.ac.jp

Editors

Reviewer #1 (Public review):

Summary:

This manuscript investigates the role of the neck linker in coordinating the stepping cycles of the two heads of a kinesin-1 motor. Previous studies in the field showed that kinesin walks by alternating stepping of its heads, referred to as hand-over-hand. In this stepping mechanism, the front head of a kinesin dimer must remain bound until the rear head dissociates from the microtubule, moves forward, and rebinds to the tubulin on the plus-end side of the front head. There is a large body of work done to address this question. These studies all point to the central role of the 14 amino acid extension, a neck-linker, which connects the two heads to a common stalk, in coordination of kinesin motility. In a two-head-bound state, the motor domains (heads) are oriented parallel to the microtubule, but the neck linkers are orienting toward each other, thereby, breaking the symmetry in a homodimeric motor. In addition, the neck linkers are quite short, almost stretching to their near contour length to accommodate the microtubule binding of both heads. Previous studies pointed out that either the opposing orientation or the intramolecular tension of the neck linkers coordinate the stepping cycle.

However, we still do not know which step(s) in the chemo-mechanical cycle is controlled by the neck-linker to keep the two heads out of phase. The front head gating model postulates that ATP binding to the front head is gated until the rear head detaches from the microtubule. The rear head gating model proposes that the neck linker accelerates the detachment of the rear head from the microtubule. In this study, the authors use pre-steady state kinetics and smFRET to address this question. They measured ATP binding and microtubule detachment kinetics of kinesin's catalytic domain with neck linker constraints 1) imposed by disulfide crosslinking of the neck linker in monomeric kinesin in backward (rear head-like) and forward (front head-like) orientations, and 2) using the E236A-WT heterodimer to create a two-head microtubule-bound state with the mutant and WT heads occupying the rear and front positions respectively. They found that neck-linker conformation of the rear head reduces the ATP dissociation rate but has little effect on microtubule affinity. In comparison, the neck-linker conformation of the front head does not change ATP binding to the front head, but it reduces ATP-induced detachment of the front head, suggesting that a step after ATP binding (i.e. ATP hydrolysis or Pi release) is gated in the front head.

Significance:

I believe that this work will make an important contribution to the large body of literature focused on the mechanism of kinesin, which serves as an excellent model system to understand the kinetics and mechanics of a molecular motor. The mechanism proposed by the authors modifies the front-head gating model and is in agreement with recent structural work done on a kinesin dimer bound to a microtubule. Overall, the work is well performed, and the conclusions are well supported by the experimental data.

https://doi.org/10.7554/eLife.106228.1.sa3

Reviewer #2 (Public review):

Summary:

In this study, the authors investigate the molecular mechanism behind kinesin-1's coordinated movement along microtubules, with a focus on how ATP binding, hydrolysis, and microtubule attachment/detachment are regulated in the leading and trailing heads. Using pre-steady state kinetics and single-molecule assays, they show that the neck linker's conformation modulates nucleotide affinity and detachment rates in each head differently, establishing an asynchronous chemo-mechanical cycle that prevents simultaneous detachment. Supported by cryo-EM structural data, their findings suggest that strain-induced conformational changes in the nucleotide-binding pockets are crucial for kinesin's hand-over-hand movement, presenting a detailed kinetic model of its stepping mechanism. The manuscript is well-crafted, technically rigorous, and should be of significant interest to cell biology and cytoskeletal motor researchers.

Significance:

All conclusions are well-supported by the provided data. The findings address a critical gap in our understanding of how kinesin's two motor domains coordinate their movements, offering insights into the molecular basis of its stepping mechanism. This work should be of significant interest to the cytoskeletal research community.

Comments on latest version:

The authors have satisfactorily addressed my comments, although I recommend the addition of the following reference:

Lu Rao, Jan O. Wirth, Jessica Matthias, and Arne Gennerich. 2025. A Two-Heads-Bound State Drives KIF1A Superprocessivity. bioRxiv 2025.01.14.632505

This paper provides conclusive evidence that kinesin-1 predominantly adopts a one-head-bound state at limiting ATP concentrations and remains in this state for a significant portion of its enzymatic cycle even at saturating ATP. This limits its processivity compared to KIF1A, which predominantly adopts a two-heads-bound state under saturating ATP conditions. These findings directly support the authors' conclusion that trailing head dissociation is favored over leading head detachment.

https://doi.org/10.7554/eLife.106228.1.sa2

Reviewer #3 (Public review):

Kinesin-1 is a dimeric motor protein that transports cargo along microtubules. Its movement relies on the ability of its two catalytic motor domains (heads) to couple microtubule interactions with directional conformational changes and ATP turnover in a coordinated,

alternating manner. The kinetics of these processes in each head are tightly regulated (gated) to ensure that at least one motor domain remains bound to the microtubule at all times, preventing detachment.

Niitani et al. investigated the gating mechanism by focusing on the role of the neck linker, a flexible region extending from the motor domain's C-terminus that undergoes conformational changes during stepping. They examined how the neck linker differentially regulates the microtubule affinity and ATP turnover of the front and rear heads. To do this, they designed cross-linkable monomeric motor domains mimicking the conformations of the front and rear heads and employed a combination of pre-steady-state and single-molecule analyses to measure ATP-binding and microtubule-detachment kinetics. Additionally, they studied a kinesin heterodimer with a locked rear head conformation to distinguish the kinetic properties of the front and rear heads within an active dimer.

ATP binding rates were measured using stopped-flow experiments with mant-ATP and nucleotide-free kinesin-microtubule complexes. The results showed that crosslinking the neck linker in the forward-pointing conformation (mimicking the rear head) reduced the ATP dissociation rate, while crosslinking it in the rear-pointing conformation (mimicking the front head) had no significant effect on ATP binding kinetics. ATP dissociation from the rear head was further examined using a kinesin mutant (E236A) that stabilizes the ATP-bound state by significantly slowing ATP hydrolysis.

To assess how neck-linker orientation affects microtubule attachment, the authors monitored turbidity changes after rapidly mixing nucleotide-free, crosslinked kinesin-microtubule complexes with ATP in a stopped-flow apparatus. Their findings demonstrated that the forward-oriented neck linker in the rear head promotes microtubule detachment, whereas the backward-oriented neck linker in the front head reduces detachment rates.

These results indicate that neck-linker conformation governs gating of microtubule affinity and nucleotide binding. Moreover, they show that even partial docking of the neck linker onto the head is sufficient to partially open the gating mechanism. To further investigate the role of neck linker tension, the authors created kinesin dimers with neck linker insertions of varying lengths. Microtubule detachment kinetics and ATPase activity assays revealed that ATP turnover in the rear head is significantly affected by the degree of forward tension applied to its neck linker.

Overall, Niitani et al. build upon previous kinesin gating models by introducing a neck-linker tension-based ATP binding affinity mechanism. Their findings provide a mechanistic basis for recent cryo-EM observations for kinesin-1 and kinesin-3 (KIF14) and distinguish the specific roles of neck linker tension in the front and rear heads in regulating ATP binding, hydrolysis, and microtubule detachment. This study is biochemically rigorous and makes an important contribution, though direct structural validation (e.g., cryo-EM snapshots of crosslinked or mutant kinesins bound to microtubules) would further strengthen their conclusions and clarify the asymmetry in ATP affinity between the front and rear heads.

https://doi.org/10.7554/eLife.106228.1.sa1

Author response:

We thank the reviewers for the detailed evaluations and thoughtful comments, which have improved the clarity and readability of this manuscript. We have responded to all reviewer comments and incorporated their suggested changes into the text and figures. We have also included new experimental results suggested by reviewer 2, which further strengthen our main conclusion.

Point-by-point description of the revisions

> ***Reviewer #1:***
>
> *(1) Introduction, page 3: The statement "Single dimeric kinesin moves processively along microtubules in a hand-over-hand manner by alternately moving the two heads in an 8-nm step toward the plus-end of the microtubule" is inaccurate. The kinesin heads take ~16 nm steps, while the center of mass advances in ~8 nm increments. Please adjust the wording accordingly.*
>
> *(2) Introduction, page 5: In the sentence "These results are consistent with the closed and open conformations of the nucleotide-binding pocket in the rear and front heads of microtubule-bound kinesin dimers observed in cryo-electron microscopy (cryo-EM) studies," I recommend changing the order to align with the previous sentence. The correct order would be "These results are consistent with the open and closed conformations of the nucleotide-binding pocket in the front and rear heads."*

We thank the reviewer for pointing out our misunderstandings. We have corrected these sentences accordingly (lines 45-47 and lines 111-112).

> ***Reviewer #2:***
>
> *MAJOR CONCERNS*
>
> *Limitations of this study: The authors need to discuss the limitations of their work. 1) They used a cys-lite kinesins mutant and introduced new surface-exposed cysteines. These mutants have lower kcat values than WT. 2) They used fluorescently labeled ATP molecules, which are hydrolyzed 10 times slower than unlabeled nucleotides. 3) They still observe crosslinking under reducing conditions and partial (but almost complete) crosslinking under oxidized conditions. 4)They assumed that cysteine crosslinked orientation mimics the orientation of the neck-linker in the front and rear conditions. The authors clearly pointed to these issues in the Results section. While these assumptions are also supported by several control experiments, the authors need to acknowledge some of these limitations in the Discussion as well.*

We have now reiterated some of the key caveats in the Discussion, and newly described in the Results section those points not mentioned in the original manuscript that do not affect the conclusion. We also added a summary of the limitations and caveats into the first paragraph of the Discussion section (lines 425-431).

(1) We added a sentence in the Results section to describe that the ATP-binding kinetics of the Cys-light mutant remained consistent with previous studies as follows: “First, we demonstrated that k_{+1} and k_{-1} of the wild-type head without Cys-modification were unchanged after oxidization (Table 1) and were comparable to those previously reported (Cross, 2004)” (lines 163-166). The reduced kcat values of cysteine pair-added mutants before crosslinking were primarily due to reduced microtubule association rate (data not included in this manuscript). We have added a sentence in the Results section describing the kcat results as follows: “The reduced ATPase activity primarily results from a decreased microtubule association rate (data to be presented elsewhere) with little change in ATP binding or microtubule dissociation rates (Table 1).” (lines 144-146).

(2) Fluorescently-labeled ATP was used to determine the ATP off-rates of the E236A mutant monomer and E236A rear head of the E236A/WT heterodimer. Two caveats in these measurements could lead to underestimating the ATP off-rate: 1) The off rate of Alexa-ATP from the head may be reduced compared to unmodified ATP, as Alexa-ATP driven motility

showed a 10-fold reduce velocity. 2) The ATP off-rate of the E236A mutant may differ from that of the rear head in the wild-type dimer, since the E236A mutant likely stabilizes the neck linker-docked state more strongly than in the rear head of the wild-type dimer. These points are crucial for evaluating the results of ATP off-rate and the affinity for ATP, so we have added sentences in the Discussion section as follows: “We note, however, that this K_d of ATP may somewhat underestimate the true value in wild-type kinesin for two reasons: first, the E236A mutation likely stabilizes the neck linker-docked, closed state more than in the rear head of the wild-type dimer (Rice et al., 1999), and second, the Alexa-ATP used to measure the ATP off-rate of E236A head showed ~10-fold smaller velocity compared to unmodified ATP, partly due to a slower ATP off-rate (Figure 2-figure supplement 3).” (lines 449-454).

(3) Under reducing condition, the rear head crosslink contained 30% crosslinked species, while under oxidized condition, the front head crosslink contained 11% un-crosslinked species (Figure 1-figure supplement 1). These heterogeneities likely affect the rate constants of K_{-1} for rear head crosslink and K_2 for front head crosslink, as crosslinked and un-crosslinked species showed significantly different rate constants. However, we did not use the rear head crosslink result to determine K_{-1}, since ATP hydrolysis likely occurred before reversible ATP dissociation. Instead, we used E236A monomer to estimate the K_{-1} of the rear head. In addition, the result for K_2 of the front head crosslink was further validated using the E236A/WT heterodimer, which will be described in the next section.

(4) This is an important point, and therefore, we conducted experiments using the E236A/WT heterodimer (including new experimental results of ATP binding kinetics of the front head) and obtained consistent results. To address this point, we have revised the following sentences in the Discussion: “In the front head, backward orientation of the neck linker has little effect on ATP binding and dissociation rates, both when measured for a monomer crosslink (Figure 2A, B) and for the front head of a E236A-WT heterodimer (Figure 4B, C, F).” (lines 432-433); “However, we found that the ATP-induced detachment rates from microtubule (K_2) were similarly reduced for both the front head crosslink (7.0 s^{-1}; Figure 3A) and the front WT head of the E236A/WT heterodimer (6.3 s^{-1}; Figures 6D), suggesting that a step subsequent to ATP binding is gated in the front head.” (lines 437-441).

> *Line 238, the authors wrote that "forward constraint on the neck linker in the rear head does not significantly accelerate the detachment from the microtubule." Can the authors comment on why the read-head-like construct has a low affinity for microtubules even in the absence of ATP (Line 220)? I believe that the low affinity of the head in this conformation is more striking (and potentially more important) than the changes they observe in detachment rates. The authors should also consider that they might not be able to reliably measure the changes in the dissociation rate in single molecule assays of this construct (especially if the release rate of the rear head in the oxidized condition increases a lot higher than that of WT). The kymographs show infrequent and brief events, which raises doubts about how reliably they can measure the release rates under those imaging conditions. Higher motor concentrations and faster imaging rates may address this concern.*

The low microtubule affinity of the rear-head-like crosslink stems from an extremely slow ADP release rate upon microtubule binding, not from a fast microtubule-detachment rate. Using stopped-flow measurements of microtubule-binding kinetics (microtubule-stimulated mant-ADP release and microtubule association rates), we found that the rear-head-crosslink resulted in a 2,000-fold decrease in the microtubule-stimulated ADP-release rate. This finding also explains the reduced ATPase of the rear-head-crosslink (Figure 1E). Since this low microtubule-affinity state occurs in the ADP-bound state rather than the ATP-bound state, we hypothesized that the neck-linker docked ADP-bound state cannot effectively bind to microtubules, requiring neck-linker undocking for microtubule binding (Mattson-Hoss et al., Proc. Natl. Acad. Sci., 111, 7000-7005 (2014)). While we acknowledge that understanding slow

microtubule binding in the neck linker docked state is important for elucidating the mechanism and regulation of microtubule-binding of the head, this paper focuses specifically on the mechanism and regulation of "microtubule-detachment". We plan to present these microtubule-binding kinetics data in a separate manuscript currently in preparation.

To explain the low microtubule affinity of the rear-head-crosslink, we added this explanation to the text; "because this constraint on the neck linker dramatically reduces the microtubule-activated ADP release rate (data to be presented elsewhere), creating a weak microtubule binding state" (lines 226-228).

Although the rear head crosslinking construct under oxidative condition showed fewer fluorescent spots per kymographs (images) due to its low microtubule binding rate, we collected more than one hundred spots by recording additional microscope movies (N=140; Figure 3-figure supplement 2B), ensuring sufficient data for statistical analysis.

> *Figure 2: How do the rates shown in Figure 2A-B compare to the previous kinetics studies in the field? The authors compare the dissociation rate of WT measured in rapid mixing experiments to that of E236A in smFRET assays. It is not clear whether these comparisons can be made reliably using different assays. Can the authors perform rapid mixing of E236A or try to determine the rate for the WT from smFRET trajectories?*

The results of ATP on/off rates are comparable to the previous stopped flow measurements of ATP binding to monomeric kinesin-1 on microtubule, which are 2-5 $\mu M^{-1}s^{-1}$ and ~150 s^{-1}, respectively (summarized in the review by Cross (2004)). We added a sentence as follows: "First, we demonstrated that K_{+1} and K_{-1} of the wild-type head without Cys-modification were unchanged after oxidization (Table 1) and were comparable to those previously reported (Cross, 2004)." (lines 163-166).

As the reviewer pointed out, the rapid mixing and smFRET data cannot be directly compared due to the differences in temporal resolution and fluorescent probe used. In Figure 2E (2F in the revised version), we measured ATP dissociation rate for both WT and E236A using smFRET. Due to the lower temporal resolution, we could not accurately determine ATP binding rate using smFRET. Therefore, to compare the ATP binding rate between WT and E236A heads, we now have added stopped-flow measurements of mant-ATP binding to the E236A monomer, as shown in Fig. 2C and Figure 2-supplement 2, and described in the text (lines 182-185).

> *Line 396: One of the most significant conclusions of this work is that the backward orientation of the neck linker has little effect on ATP binding to the front head. This is only supported by the results shown in Fig. 2A-B. Can the authors perform/analyze smFRET assays on the E236A/WT heterodimer to directly show whether the ATP binding rate to the WT head is affected or not affected by the orientation of the neck linker of the WT head?*

We agree with the reviewer that our finding about ATP binding to the front head is potentially significant in the kinesin field, as it has been widely believed that ATP-binding is suppressed in the front head. In our original manuscript, this conclusion was supported only by the measurement of ATP on-rate of the front-head-crosslink, which may differ from the front head of a dimer in which the backward orientation of the neck linker is maintained by the backward strain. Although the reviewer suggested performing smFRET experiments using E236A/WT heterodimer, smFRET have relatively low temporal resolution (50-100 fps) and cannot accurately measure the frequency of ATP binding, so we used this technique only to determine ATP off rates. In this revised manuscript, we now have added stopped-flow experiments to separately measure the ATP binding to the front and rear heads of the E236A/WT heterodimer. By labeling the rear E236A head with a fluorophore to quench the

mant-ATP signal bound to the rear head, we successfully measured mant-ATP binding rate to the front head. We found that the ATP-binding rate to the front head was comparable to that of an unconstrained monomer head, providing direct evidence for our conclusion. The revised version includes Fig. 4 A-C (with Figure 4-supplement 2; Figs. 4 and 5 are swapped in order) showing the kinetics of ATP binding to the front and rear heads of the E236A/WT heterodimer, with corresponding text in the result section (lines 315-324).

> *MINOR CONCERNS*
>
> *Lines 31 and 32: I recommend replacing "ATP affinity" with "ATP binding rate" or "the dissociation of ATP" to be more specific. This is because they do not directly measure the affinity (Kd), but instead measure the on or off rates.*
>
> *Line 41: Replace "cellar" with "cellular".*
>
> *Line 83: The authors should cite Andreasson et al. here.*

We have corrected these sentences accordingly (lines 31, 40, 85).

> *Lines 83-86: It seems this sentence belongs to the next paragraph. It also needs a citation(s).*

This statement lacks experimental evidence and may confuse readers, so we have removed it for clarity.

> *Line 151: It would be helpful to add a conclusion sentence at the end of this paragraph to explain what these results mean to the reader.*

A conclusion sentence of this paragraph has been added: “These results demonstrate that neck linker constraints in both forward and rearward orientations inhibit specific steps in the mechanochemical cycle of the head (lines 151-153)”.

> *Lines 175-180: I recommend combining and shortening these sentences, as follows, to avoid confusing the reader: "To detect the ATP dissociation event of the rear head, we employed a mutant kinesin with a point mutation of E236A in the switch II loop, which almost abolishes ATPase hydrolysis and traps in the microtubule-bound, neck-linker docked state,"*

We have corrected these sentences accordingly (line 179-181).

> *Line 314: "which was rarely observed ...". This is out of place and confusing as is. I recommend moving this sentence after the sentence that ends in Line 295.*

This sentence explains how the dark-field microscopy data was analyzed to determine whether the labeled head was in the leading or trailing position before detaching from the microtubule, but the explanation needs clarification. We removed the phrase “which was rarely observed for E236A-WT heterodimer” and simplified this sentence as follows: “Moreover, these observations allow us to distinguish whether the gold-labeled WT head was in the leading or trailing position just before microtubule detachment; the backward displacement of the detached head indicates that the labeled WT head occupied the leading position prior to detachment (Figure 5-figure supplement 1).” (lines 347-351).

> *Line 300: Can the authors comment on why E236A/WT has a substantially lower ATPase rate than WT homodimer? Is it possible to determine which step in the catalytic cycle is inhibited?*

We demonstrated that the k_2 (microtubule-detachment rate) of the front head matched the ATP turnover rate of the E236A/WT heterodimer (Figure 6 B and E), suggesting that the inhibited step occurs after ATP binding in the front head. In contrast, the rear E236A head showed virtually no ATP hydrolysis activity, since in high-speed dark field microscopy, we observed forward step caused by rear E236A head detachment from microtubule only rarely, approximately once every few seconds (Figure 5-figure supplement 1). We added a sentence in the text as follows: “As described later, the reduced ATPase rate results from suppressed microtubule detachment of the front WT head, while the rear E236A head is virtually unable to detach from microtubules” (lines 311-313).

> *Line 323: Is the unbound dwell time unchanged?*

The unbound dwell time exhibited a weak ATP-dependence, which we described only in Figure 5-supplement 2 (Figure 4-supplement 2 in the old version). We observed three distinct phases in the unbound dwell time based on mobility differences, with ATP dependence appearing only in the third phase. This finding suggests that ATP binding to the microtubule-bound E236A head is sometimes necessary for the detached WT head to rebind to the forward-tubulin binding site, indicating that the microtubule-bound E236A head occasionally releases ATP during the one-head-bound state (without the forward neck linker strain). To describe the ATP-dependence of the unbound dwell time, we added a sentence in the main text as follows: “In contrast, the dwell time of the unbound state of the gold-labeled WT head showed weak ATP dependence (Figure 5-figure supplement 2), indicating that the rear E236A head occasionally releases ATP when the front head detaches from the microtubule and the neck linker of E236A head becomes unconstrainted. This finding further supports the idea that forward neck linker strain plays a crucial role in reducing the reversible ATP release rate.” (lines 372-377).

> *Line 331: I recommend replacing "ATP-induced detachment" with "nucleotide-induced detachment" for clarity.*

We have revised the phrase accordingly (line 371).

> *Line 344: I recommend replacing "affinity" with "forward strain prevents the release of the nucleotide" or similar to avoid confusion. Forward strain reduces the off-rate of the bound nucleotide, rather than allowing ATP to bind more efficiently to the rear head.*

We agree to the reviewer’s comment and have corrected this sentence accordingly (line 338).

> *Lines 376-385: G7-12 constructs are introduced in Figure 6, but the results in this paragraph are shown in Figure 5. They should be moved to Figure 6 to avoid confusion.*

To improve the readability, we have reorganized Figures 4-6, such that all the figure panels related to the neck linker extended mutants are shown in Figure 6; Figure 5D has been moved to Figure 6F.

> *Line 421: delete "not" before "does not".*

We have corrected this typo.

> *Lines 433-441: Unless I am mistaken, more recent work in the kinesin field showed that backward trajectories of kinesin 1 reported by Carter and Cross are due to slips from the microtubule rather than backward processive runs of the motor.*

The slip motion demonstrated by Sudhakar et al. (2021) differs from the backstep motion reported by Carter and Cross (and many other laboratories). Slip motion occurs after kinesin detaches from the microtubule and continues until the bead returns to the trap center. In contrast, backstep motion occurs during processive movement when the trap force either exceeds or approaches the stall force. The kinetics of these motions also differ significantly: slip steps occur with a dwell time of 71 μs and are independent of ATP concentration, while backsteps take ~0.3 s (at 1 mM ATP) and depend on ATP concentration. These differences indicate that slip motion is phenomenologically distinct from backsteps occurring under supra-stall or near-stall force.

> *Line 474: Replace "suppresses" with "suppressed".*

We have corrected this typo.

> *Figure 4E: I would plot these results with increasing ATP concentration on the x-axis.*

We formatted Figure 4E to match Figure 4b from Isojima et al. (Nature Chem. Biol. 2015), to emphasize the difference in ATP dependence of the front and rear head.

> *Figure 4B: The authors should explain how they distinguish between bound and unbound states in the main text or figure legends. For example, it is not clear how the authors score when the motor rebinds to the microtubule in the first unbinding event shown in Figure 4B (displacement plot).*

The method was described in the Materials and Methods section, but we have now described how to distinguish between bound and unbound states in the main text as follows: “Unlike the unbound trailing head of wild-type dimer that showed continuous mobility (Isojima et al., 2016), the unbound WT head of E236A-WT heterodimer exhibited a low-fluctuation state in the middle (Figure 5B, s.d. trace). This low-fluctuation unbound state was distinguishable from the typical microtubule-bound state, having a shorter dwell time of ~5 ms compared to the bound state and positioning backward, closer to the E236A head, relative to the bound state (Figure 5-figure supplement 2).” (lines 351-356).

> ***Reviewer #3:***
>
> *Minor Issues:*
>
> *- Line 22, Abstract - The phrase "move in a hand-over-hand manner" could be clearer if phrased as "move in a hand-over-hand fashion" to improve readability.*

We changed the word “manner” to “process” (line 23).

> *- Abstract - Neck linker conformation in the leading head: The sentence "We demonstrate that the neck linker conformation in the leading kinesin head increases microtubule affinity without altering ATP affinity" would benefit from defining this conformation as "backward" for clarity.*
>
> *- Abstract - Neck linker conformation in the trailing head: The sentence "The neck linker conformation in the trailing kinesin head increases ATP affinity by several thousand-fold compared to the leading head, with minimal impact on microtubule affinity" should also clarify that this conformation is "forward."*

We have corrected these sentences accordingly (line 30, 32).

> *- Abstract - Conformation-specific effects: The authors mention conformation-specific effects in the neck linker structure but do not define the neck linker's conformation or the motor domain's (MD) conformation. Clarifying these conformational changes would improve the explanation of how they promote ATP hydrolysis and dissociation of the trailing head before the leading head detaches from the microtubule, thereby providing a kinetic basis for kinesin's coordinated walking mechanism.*

We have revised the last sentence of the abstract accordingly by specifying the neck linker's conformation as follows: "In combination, these conformation-specific effects of the neck linker favor ATP hydrolysis and dissociation of the rear head prior to microtubule detachment of the front head, thereby providing a kinetic explanation for the coordinated walking mechanism of dimeric kinesin." (lines 34-37).

> *- Line 306 - Use of ATP in the E236A-WT heterodimer: In discussing the "ATP-induced detachment rate of the WT head in the E236A-WT heterodimer," the authors should consider justifying their choice of ATP over ADP for inducing microtubule (MT) dissociation. Since ATP typically promotes tighter MT binding and ATP turnover is reduced in forward-positioned WT heads, it may be unclear to some readers why ATP was chosen.*

We measured the ATP-induced detachment rate k_2 of the front head of the E236A-WT heterodimer to validate our findings from the front-head-crosslinked monomer experiments, which demonstrated reduced k_2 after oxidation. To clarify this point, we have now included ATP binding kinetics measurements for both front and rear heads of the E236A-WT heterodimer, as suggested by reviewer 2. These additional data demonstrate consistency between the results from the crosslinked monomer and E236A-WT heterodimer experiments.

> *- Discussion - Backward-oriented neck linker in the front head: The discussion mentions that the backward-oriented neck linker in the front head reduces its ATP-induced detachment rate, suggesting that a step after ATP binding (e.g., isomerization, ATP hydrolysis, or phosphate release) is gated in the front head. However, the authors do not clarify that the backward neck linker orientation would imply the nucleotide pocket should be open or at least not fully closed, thus inhibiting ATP turnover. This is important because, as demonstrated in other studies, full closure of the nucleotide pocket is linked to neck linker docking. This point should be addressed earlier in the discussion.*

We have addressed this point by revising this sentence as follows: "These results are consistent with an inability of the front head to fully close its nucleotide pocket to promote ATP hydrolysis and Pi release (Benoit et al., 2023), as will be discussed later." (lines 441-443)

https://doi.org/10.7554/eLife.106228.1.sa0